

Invited Research Article

Building an inversely zoned post-orogenic intrusion in the Neoproterozoic-Cambrian Araçuaí orogen (Brazil)

U.D. Bellon^{a,*}, M.S. D'Agrella-Filho^a, F.A. Temporim^a, G.F. Souza Junior^a, C.C.V. Soares^b, C.A. D. Amaral^a, L.P. Gouvêa^c, R.I.F. Trindade^a

^a Instituto de Astronomia, Geofísica e Ciências Atmosféricas, Departamento de Geofísica, Universidade de São Paulo, São Paulo, Brazil

^b Departamento de Geologia, Universidade Federal do Espírito Santo, Alegre, Brazil

^c Departamento de Geologia, Universidade Federal do Rio de Janeiro, Rio de Janeiro, Brazil



ARTICLE INFO

Keywords:

Araçuaí orogen
Venda nova pluton
Post-orogenic magmatism
Anisotropy of magnetic susceptibility
Inversely zoned plutons

ABSTRACT

Post-orogenic plutons are excellent recorders of the last stages of collapsing orogens. In the Neoproterozoic-Cambrian Araçuaí orogen (Brazilian Southeast), one of the Brasiliano orogenies (Western Gondwana), voluminous amounts of Cambrian magmatism crop out. The Venda Nova pluton (VN) is located at the southern portion of the AO, exhibiting a norite/charnockitic west-ring in contact with a syenomonzonite that envelops an alkali-gabbro core with distinct geochemical signatures. To explore the tectonic significance of this post-orogenic pluton in the AO, anisotropy of magnetic susceptibility (AMS) together with a microstructural analysis were performed. AMS data reveals, majorly, a concentric magnetic foliation/lineation pattern, implying that buoyancy forces controlled the magma emplacement of syenomonzonites and gabbros, while a previous pulse of a charnockitic intrusion was deformed by their intrusion. Restrict solid-state deformation (following the regional trend) inside the pluton could result of the reactivation of an emplacement structure in the last stages of VN crystallization. The emplacement of inversely zoned post-orogenic plutons through deep conduits in the colder forelands of the AO, such as the VN, might record different stages of a large collapsing orogen in a single plutonic body.

1. Introduction

Late-to-post-orogenic magmatism can involve a huge variety of geological events, such as large movements along shear zones and lithospheric delamination, including continuous or episodic extensional regimes that involve various types of magmatism (Liégeois, 1998). As felsic post-orogenic magmatism records the reworking and growth of the crust, post-orogenic mafic magmatism reflects the evolution of the orogenic mantle (Xu et al., 2020 and references therein). Studying the magnetic and magmatic fabric of such plutons allows an overview not only of how magma flows and is emplaced into the crust, but also of the regional stress regimes and strain distribution across an orogen (Archanjo and Bouchez, 1997).

The Araçuaí orogen (AO) is a Neoproterozoic belt (Fig. 1) positioned in the southeast of the São Francisco Craton (SE-Brazil), formed during the final amalgamation of the Gondwana (Almeida, 1977). It was built parallel to the southeastern margin of the Brasiliano-Pan-African Orogeny, merging at south with the Ribeira Belt (part of the

Neoproterozoic-Cambrian orogenic systems). The history of AO contemplates a wide register of magma production and emplacement (630–480 Ma) (Pedrosa-Soares et al., 2011; Gradim et al., 2014; Tedeschi et al., 2016; Melo et al., 2017). The evolution of AO is highly discussed and two main distinct models based on geothermal, geochronological, geophysical, structural and geochemical data are proposed (i) a collisional-subduction model and (ii) an intracontinental orogeny.

Although heavily studied from the geochemical/geochronological perspective, structural data of these post-orogenic plutons is still scarce, mainly because of the apparently isotropic mineral fabric (Bayer et al., 1987). However, as claimed by Bouchez (1997), “granite is never isotropic”. Studying the magnetic fabric of rocks might reveal important structural evidences, sometimes hidden from macroscopic observation, leading to important geological correlations, such as magma emplacement and tectonic deformational regimes (Bouchez et al., 1990; Borra-daile and Henry, 1996; Archanjo and Bouchez, 1997; Bouchez, 1997; Nédélec and Bouchez, 2015).

* Corresponding author.

E-mail address: ualisson.bellon@usp.br (U.D. Bellon).

<https://doi.org/10.1016/j.jsg.2021.104401>

Received 26 February 2021; Received in revised form 8 June 2021; Accepted 15 June 2021

Available online 17 June 2021

0191-8141/© 2021 Elsevier Ltd. All rights reserved.

The Venda Nova pluton (VN) crops out in the southern sector of the AO. It consists of a circular intrusion, with a gabbro-noritic core slightly shifted to the west, a syenomonzonite envelope and a norite/charnockite narrow ring bordering it (Horn and Weber-Diefenbach, 1987; Ludka et al., 1998; Mendes and De Campos, 2012). VN rocks have been interpreted as post-orogenic features due to their geochemical similarities to other Cambrian plutons in the southern Araçuaí orogen (Ludka et al., 1998) and due to the fact that its circular shape seems to contrast with the regional syn-orogenic units that are oriented in a NE-SW trend. However, this plutonic feature has unique singularities, as pointed by Mendes and de Campos (2012), such as: (i) the noritic outer rocks are tholeiitic, while the rest of the units have calc-alkaline signatures, and (ii) the external charnockitic ring shows evidence of solid-state deformation (which is apparently absent in the internal facies).

A circular shape, however, does not exclude the possibility of regional strain to be recorded in the magmatic fabric (Petitgirard et al., 2009). Recent studies of the magnetic fabric in neighbor plutonic features have shown strong anisotropy and internal solid-state deformational structures (e.g. the Santa Angelica pluton), even though geochronological data points to the period of gravitational collapse of AO (Temporim et al., 2020b). Understanding of regional tectonic stress requires a detailed mapping of structures, especially for Cambrian plutons of the AO, that shows contradictory strain distribution across the orogen (Temporim et al., 2020a).

In this paper, we aimed a detailed AMS and microstructural study to determine the emplacement mechanisms of Venda Nova units, and the

internal structural relation between its facies, as well as to find indications of the regional stress during its intrusion.

2. Geological setting

2.1. The Araçuaí orogen and the post-orogenic magmatism

One of the key-aspects of the Araçuaí orogen is the common acceptance (see Alkmim et al., 2006) that the Congo and São Francisco cratons remained connected from the Transamazonian-Eburnean collage (ca. 2 Ga) until the Mesozoic, at the opening of the Atlantic Ocean (Pedrosa-Soares et al., 2001). In the collisional-subduction model of AO, the cratonic bridge would allow the paleocontinents of South Africa and South America to remain connected during a Tonian taphrogenesis, resulting in the creation of an oceanic lithosphere and a large basin covered by the Adamastor ocean (Alkmim et al., 2006). A widely cited scenario for the next evolutionary stage, related to the formation of the orogen, would be similar to “closing of a nutcracker” mechanism, that is, the São Francisco peninsula would rotate counter-clockwise against the Congo continent, leading the basin to generalized compression and consumption of its oceanic lithosphere that would have subducted under the Congo’s side (Alkmim et al., 2007; Pedrosa-soares et al., 2007; Pedrosa-Soares et al., 2011). In this model, which represents a complete Wilson’s Cycle, magmatism have been associated to distinct tectonic-stages, i. e., pre (630 - 580 Ma), sin (580 - 560 Ma), late (560 - 530 Ma) and post-collisional magmatism (530 - 480 Ma), mainly

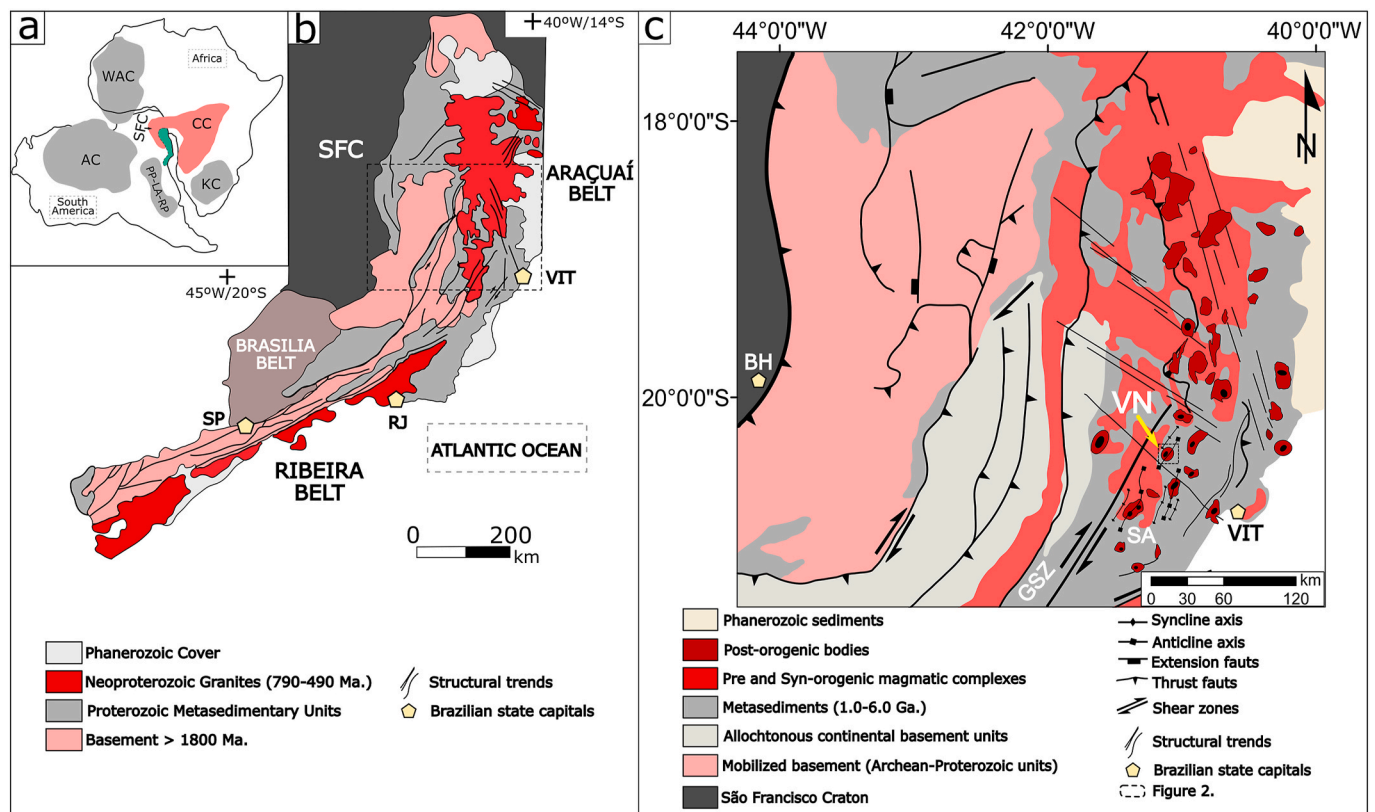


Fig. 1. Regional contextualization and general geological setting of the Araçuaí orogen. a) Geographic representation of South America and Africa in a pre-drift configuration and the major geological cratons, built mainly based on Alkmim et al. (2006). Cratonic units in gray: AC – Amazonian Craton, PP-LA-RP – Parapanema, Luiz Alves and Rio de la Plata; KC – Kalahari Craton; and WAC – West African Craton; Other cratonic units (in salmon): SFC – São Francisco Congo Craton and CC – Congo Craton. b) Segment of the Brasiliano–Pan-African Orogeny disposing some of the Neoproterozoic Belts (green in a), such as the Araçuaí, Ribeira and a portion of the Brasília orogen (modified from Alkmim, 2015). Cities: VIT – Vitória, RJ – Rio de Janeiro, SP – São Paulo, BH – Belo Horizonte. c) Section over the post-orogenic intrusion area of the Araçuaí orogen. Black ellipses inside the post-orogenic units indicate the presence of a mafic core. The dashed polygon represents the fieldwork campaign related to this paper. Anticline and syncline structures based on Bayer et al. (1987). All geological units based on Cavalcante et al. (2019) (and references therein) with exception of post-orogenic bodies (based on De Campos et al., 2016). VN – Venda Nova pluton, SA – Santa Angélica pluton, GSZ – Guaçuí shear zone. (For interpretation of the references to colour in this figure legend, the reader is referred to the Web version of this article.)

through a coherent geochemical/geochronological perspective.

However, Trompette (1997), as summoned by Cavalcante et al. (2019), have considered the Araçuaí-West-Congo Orogen “partly of totally intracratonic”, obstructing a proto-South Atlantic ocean (Adamastor Ocean) northwards. Several matters about the collisional model have been recently raised (Fossen et al., 2020; Konopásek et al., 2020), the most prominent of them is how to accommodate hundreds of kilometers of oceanic crust (consequence of the collisional-subduction model) given the lack of structures to allow such kinematics between the São Francisco and Congo cratons through the cratonic bridge. In the intracratonic model, a restrict collision – whose mobility would have been provided by the aulacogens (Fossen et al., 2017) – would result in a limited amount (or none) of oceanic crust, with a hot internal domain with intense magmatic activity as result of orogenic thickening (lasting from 620 to 580 Ma) and radioactive decay, that formed a partially molten midcrust (Cavalcante et al., 2018). Instead of thrusting sheets typical of cold subduction collisional orogens, the geomorphology of the AO would be of a large plateau, eventually collapsing gravitationally towards (channel flow) the colder forelands (Cavalcante et al., 2019).

Regardless the geotectonic model for AO evolution, voluminous amounts of intrusive Cambrian-Ordovician AO (535–480 Ma) post-orogenic bodies intrudes pre-syn-orogenic units from north to south

(Fig. 1b and c). Numerous studies have been published during the last decades, mainly on their petrology, geochronology and geochemistry (Bayer et al., 1987; Horn and Weber-Diefenbach, 1987; Ludka et al., 1998; Medeiros et al., 2000; Wiedemann et al., 2002; De Campos et al., 2004; Mendes et al., 2005; Pedrosa-soares et al., 2007; Mendes and De Campos, 2012; Tedeschi et al., 2016; Peixoto et al., 2017; Serrano et al., 2018; Araujo et al., 2020). In the northern part of the AO, where relatively upper crustal levels are exposed, Cambrian post-orogenic plutons form large, elongated N-striking bodies parallel to the belt. Amalgamated intrusions make up granitic batholiths with only subordinate mafic components (Serrano et al., 2018).

Southern AO major structures are NE-trending, dextral transpressive shear zones (Wiedemann et al., 2002 and references therein). The volume of post-orogenic magma is significantly lower and the intrusions are circular or elliptical in shape. These plutons mostly include I-type and A-type granitic rocks, and their opx-bearing charnockitic equivalents (Pedrosa-Soares and Wiedemann-Leonardos, 2000; De Campos et al., 2004, 2016). In this sector of the orogen they usually form inversely-zoned balloon-like plutons, composed of granitic-charnockitic rocks and gabbro-noritic cores, with striking magma mixing and mingling features, and chemical-isotopic evidence of mantle involvement, interpreted as results of magmatic activity in a collapsing orogeny

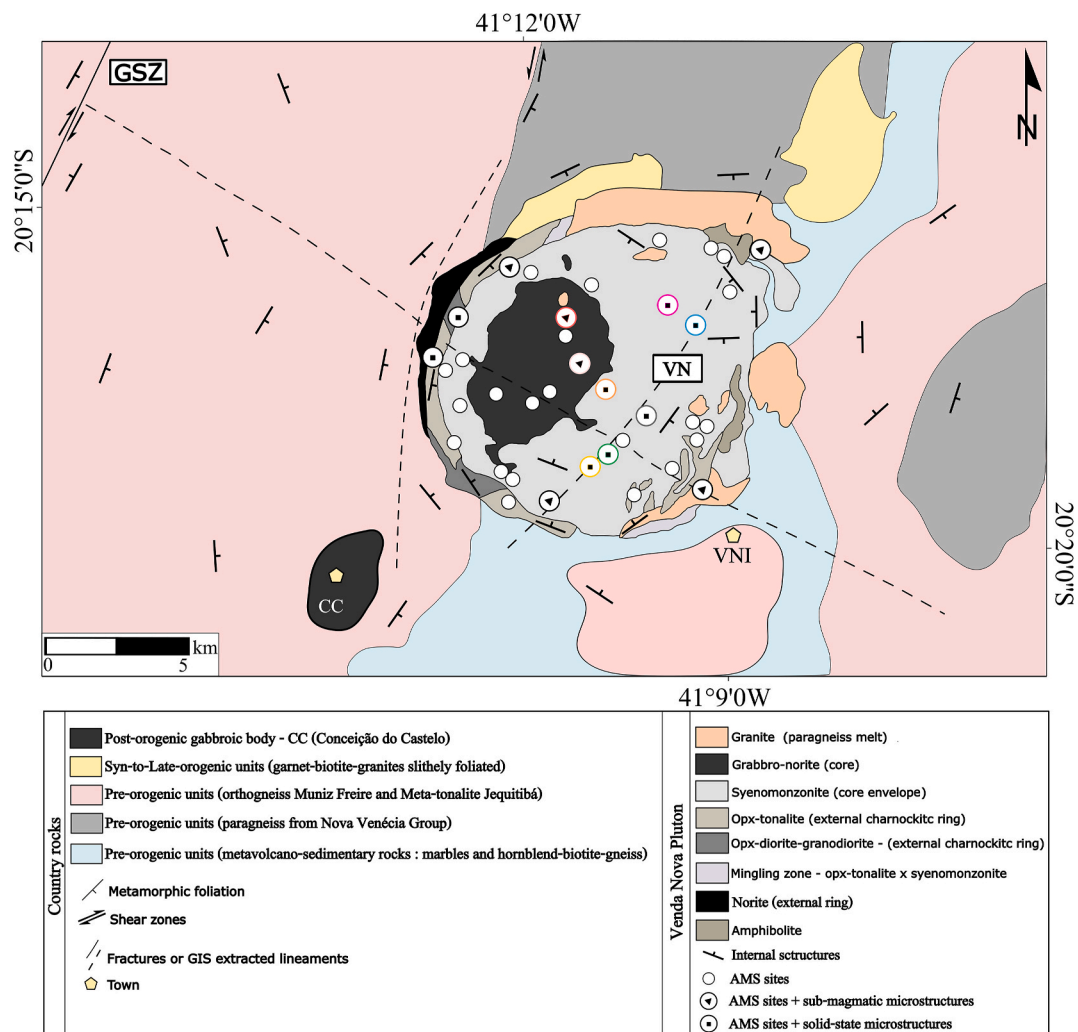


Fig. 2. Geological map of the Venda Nova pluton (VN). For the country rocks, lithological and foliation data are based, and simplified, on the Brazilian Geological Survey data (Vieira and Menezes, 2015) and from Folha Afonso Cláudio (Signorelli, 1993). Geological units of VN were modified from De Campos et al. (2016) (after Mendes & De Campos et al., 2012). Metamorphic foliation of the country rocks seems to be deflected by the intrusion. Looking on Venda Nova units, a west-shifted gabbro-norite core is surrounded by an envelope of syenomonzonitic rocks. In the west border, a “narrow ring” of charnockitic and noritic rocks partially crop out. Colored sites matches the thin sections show in this paper. Cities: CC – Conceição do Castelo, VNI – Venda Nova do Imigrante.

that could have intruded through weak zones in the crust (De Campos et al., 2004, 2016) (Fig. 1b and c).

2.2. The Venda Nova pluton (VN)

The post-orogenic suites in the Araçuaí orogen comprise granites, diorites and charnockites, exhibiting magma mixing and mingling features into inversely zoned plutons (De Campos et al., 2004, 2016). Their internal fabric might present quite evident alignment of phenocrysts indicating magmatic flow and solid-state deformation along the borders (Wiedemann et al., 2002).

According to Mendes and De Campos (2012), the VN (Fig. 2) is an elliptical structure with at least 75 km² of area with a narrow ring of charnockitic rocks partially enveloping its western side (Mendes and De Campos, 2012). It intrudes orthogneisses and paragneisses metamorphosed mainly in high-amphibolite phases. Metamorphic foliation is oriented to NE-SW with distinct degrees of dip angles. Shear zones of both dextral and sinistral movement, and regional folds seem to have served as the main conduit for the emplacement of post-orogenic plutons (Wiedemann et al., 2002). The most noticeable in the Venda Nova area is the NE-SW Guaçuí shear zone (GSZ), located less than 10 km to the north of the VN and an anticline axis that passes across the pluton and considered by Wiedemann et al. (2002) as the possible emplacement structure of the Venda Nova pluton.

Ludka et al. (1998) defined the main petrological facies of the Venda Nova (Fig. 2) distributed concentrically and recognized them as: a) syenomonzonite envelope, mainly composed of a microperthitic microcline/mesoperthite, oligoclase/andesine, biotite, hornblende and a minor accessory minerals as quartz, pyroxenes (clino and ortho), ilmenite/titano-magnetite, titanite, allanite and zircon; b) a gabbro-norite core mainly composed by labradorite, diopside, bronzite/hypersthene, biotite, hornblende, ilmenite, titanomagnetite, sulphides and olivine-pyroxene-phlogopite cumulates; c) a monzodiorite “halo” that would result from the mixing of the two other units; mantling of feldspar and pyroxene-amphibole transformations are described as preserved signs of mechanical mixing; d) granites, delimited in two major groups – a microcline granite and a fine-grained-leucogranite – both resulting from the fusion of the paragneisses country rocks.

Along the border of the Venda Nova, Mendes & De Campos (2012) recognized a norite and tonalitic to dioritic composition charnockitic ring, which is characterized and interpreted it as follows. The primary flow structures were recognized by preferred orientation of plagioclase phenocrysts and biotite. Subtle sub-solidus deformation is indicated by wavy extinction of twin lamellae and polygonal contacts. Geochemical evidence suggests that these rocks cannot be derived from the same parental magma of the syenomonzonites and gabbros, leading to the idea of an early magmatic pulse of charnockite-norite intrusion prior to the main circular intrusion with inverted zoning. Mineral chemistry in pyroxenes, feldspars, amphibole, biotite, ilmenite and magnetite indicate average igneous crystallization temperature (Opx-Cpx coexisting pairs) of 908 °C and 958 °C, for the norite and charnockite, respectively, and a pressure during crystallization (Al-in-hornblend geobarometer) ranging from 5.5 to 6.0 kbar, which would correspond to deep crustal intrusion levels at about 18–20 km. Seismological data of Assumpção et al. (2013) shows that AO southern portion crust has a current thickness of ≈40 km. Considering the geobarometric data of Mendes and De Campos (2012), the VN pluton should have intruded through a crust of nearly 60 km.

2.3. Sampling and field observations

Oriented core samples were extracted from 36 sites evenly spaced across the pluton (Fig. 2). Lithologies and geographic coordinates are described in Table 1. At least 8 cores were drilled at each site using an adapted gasoline powered portable drill. Each core is ca. 7–8 cm in length and about 2.5 cm in diameter, and was oriented to solar and

magnetic compass.

Contacts between the intrusion and the country rocks are subvertical, and the foliation at the border of the pluton is parallel to the contact with the country rocks. The country rocks close to the border of the Venda Nova are intensively deformed, where gneisses have west-vergence isoclinal folds (Fig. 3b) in the southern border and intense ductile deformation features in the northern border (Fig. 3c). At distances greater than 5 km from the contact with the country rock, the foliation is concordant with the regional NE-SW structural trend. This foliation dips toward the interior of the intrusion with the dip angle increasing closer to the pluton. Near the NW border, quartz boudins along the vertical foliation of mylonitic rocks show a dextral shear sense (Fig. 3d).

Four sites were sampled in the west-charnockitic ring. Its major geomorphology is of hills of hundreds of meters in amplitude, usually well preserved or showing a few centimeters of an intemperized cover. Charnockites were found to be mostly porphyritic, sometimes defining a magmatic flow that dips towards the syenomonzonites. Syenitic dikes cut this unit and show intense dynamical deformational features, such as porphyroclastic alkali-feldspar with dextral cinematics (Fig. 3a). The syenomonzonite unit dominates the relief in the VN, allowing 23 sites to be sampled. These rocks crop out mostly as huge convex-like monoliths harnessed by dimensional stone mining for its apparent isotropy and low occurrence of intemperic features, affording sampling sites of dozens of meters in extension. No direct contact between the border charnockites and the syenomonzonite was found. Contrastingly, the shifted gabbroic core represents a topographic low in the VN. Gabbroic rocks usually appear as outcrops of a few meters in extension near water streams, which limited the sampling sites to 8. Although Ludka et al. (1998) considered the syenomonzonites and the gabbroic core essentially contemporaneous marked by gradational transition with hybrid rocks in-between, abrupt contact between these units can also be found in the southernmost portion of the gabbro (Fig. 3e). Samples collected exactly at these abrupt contacts clearly reveal the thin granulation of the mafic portion, almost aphanitic, and the large feldspar grains from the syenomonzonite envelope (Fig. 3f). In the NW portion of the VN, gabbroic dikes section the syenomonzonite unit. Although these dikes have well defined edges, both mingling and mixing strips are found (Fig. 3g) forming strips inside the dike's body.

3. Methods

To avoid shape anisotropy errors caused by the external geometry, the cores were cut into specimens with 2.2 cm in length, resulting in a total of 600 samples. The whole process of preparation and measurements of the samples was performed in the Laboratório de Paleomagnetismo of Universidade de São Paulo (USPmag).

The anisotropy of magnetic susceptibility (AMS) provides a semi-quantitative fabric description of magmatic rocks (Bouchez, 1997). The AMS of a site can be understood as a second-rank symmetrical tensor with K_1 , K_2 and K_3 defining an ellipsoid of orthogonal axes, interpreted as the three principal susceptibilities for which K_1 (max) > K_2 (int) > K_3 (min). Direct information of magnetic lineation is found by looking at the K_1 axis, whereas K_3 axis indicates the pole of the magnetic foliation – those considered equivalent to the rock's lineation and plane of foliation, respectively, if the magnetic fabric is normal (Bouchez, 1997). Some parameters, as shown by Jelínek (1978), provide information about the shape and structure of the rocks. Evaluating the degree of anisotropy ($P = K_1 * K_3^{-1}$) clarifies if the sample is isotropic ($P = 1$) or how much anisotropic it is as P increases. One can also investigate the shape of the ellipsoids by means of the shape factor (Jelínek parameter, T), which is defined as $2 * \ln(K_2 * K_3^{-1}) / \ln(K_1 * K_3^{-1}) - 1$. It varies from -1 for prolate, purely linear magnetic fabric (i.e. $K_1 \gg K_2 \approx K_3$) through 0 (neutral) to $+1$ for oblate, purely planar magnetic fabric (i.e. $K_1 = K_2 \gg K_3$). The AMS of each individual specimen was measured with an Agico Kappabridge MFK 1A. Mean values of K_1 , K_2 and K_3 per site were obtained through the statistical methodology of Jelínek (1978)

Table 1
Anisotropy of magnetic susceptibility parameters of the Venda Nova*.

Sites	N	Geographical Coordinates		Magnetic Parameters			Main axis directions					
		Lat	Lon	K SI (mean)	P	T	K ₁ (dec/inc)	ε ₁₂ (K ₁)	K ₂ (dec/inc)	ε ₂₃ (K ₂)	K ₃ (dec/inc)	ε ₃₁ (K ₃)
Granite												
VNU1	10	-20°19'04.08"	-41°09'27.38"	0.1050 ± 0.018	1.324	-0.129	323.5/74.0	8.3/3.1	56.4/0.8	6.8/3.9	146.6/16.0	7.9/6.3
Syenomonzonites												
VNU2	8	-20°19'10.04"	-41°10'26.67"	0.1416 ± 0.022	1.202	0.322	354.9/61.6	7.4/2.9	240.3/12.73	11.2/6.6	144.3/24.9	10.8/3.1
VNU3	6	-20°18'38.21"	-41°10'52.83"	0.0781 ± 0.014	1.095	-0.033	230.8/2.1	16.5/9.6	326.4/39.9	27.1/19.0	136.8/61.8	18/1.5
VNU4	10	-20°18'24.87"	-41°10'35.42"	0.0435 ± 0.012	1.084	-0.531	231.3/15.9	25.1/11.7	335.9/41.4	47.2/21.7	125.2/44.3	47.2/13.7
VNU6	8	-20°17'18.46"	-41°13'14.55"	0.0666 ± 0.022	1.136	0.449	120.8/57.1	21.3/10.9	4.9/15.8	27.8/8.4	266.2/28.0	12.1/5.8
VNU9	10	-20°16'03.72"	-41°11'04.76"	0.0250 ± 0.007	1.103	0.288	292.3/8.7	20.1/7.8	33.7/51.2	24.1/12.1	194.9/32.1	15.6/6.9
VNU10	10	-20°15'54.11"	-41°11'56.21"	0.0460 ± 0.016	1.022	0.210	85.6/52.0	55.4/43.8	262.0/38.0	53.6/50.8	353.4/1.8	54.3/43.5
VNU11	11	-20°18'22.55"	-41°09'30.94"	0.1030 ± 0.019	1.216	-0.098	308.0/58.0	10.0/4.1	39.7/1.0	10.8/7.5	130.3/8.8	8.8/4.1
VNU12	9	-20°18'07.56"	-41°09'28.21"	0.0650 ± 0.015	1.163	0.223	299.5/65	13/11.2	43.3/6.4	13.9/11.3	136.2/24.1	15.6/6.3
VNU13	9	-20°18'08.52"	-41°09'23.95"	0.0722 ± 0.018	1.107	-0.007	21.1/26.4	15.2/7.8	259.7/46.4	19.6/13.6	129.1/31.8	19.4/10.1
VNU14	9	-20°16'10.71"	-41°09'01.24"	0.0713 ± 0.020	1.147	-0.745	261.2/59.2	7.2/5.2	146.5/14.0	34.6/6.6	49.3/26.8	34.6/5.7
VNU15	10	-20°15'38.45"	-41°09'10.30"	0.1020 ± 0.024	1.102	-0.147	232.0/71.0	8.7/4.5	63.0/18.7	14.2/6.6	331.9/3.4	13.6/5.6
VNU16	17	-20°15'35.05"	-41°09'14.59"	0.0960 ± 0.013	1.125	-0.448	209.2/64.1	9.1/4.8	69.0/20.4	26.5/6.4	333.2/15.2	23.0/7.5
VNU18	7	-20°15'23.17"	-41°08'43.35"	0.0996 ± 0.010	1.230	-0.573	228.3/57.5	8.1/2.9	123.9/9.0	13.6/2.9	28.4/30.9	14.3/3.5
VNU19	8	-20°15'26.02"	-41°10'03.53"	0.0983 ± 0.016	1.136	-0.287	211.3/72.2	15.8/8.4	115.8/1.8	23.7/10.7	25.2/17.7	24.0/5.7
VNU20	5	-20°15'51.11"	-41°12'17.32"	0.0606 ± 0.036	1.084	-0.044	34.3/20.7	13.2/10.4	274.9/52.4	23.0/11.6	136.8/29.8	24.3/8.1
VNU21	7	-20°17'11.72"	-41°12'57.36"	0.0369 ± 0.010	1.107	0.372	167.5/45.8	15.2/6.8	55.1/20.3	19.7/10.7	308.8/37.2	17.3/6
VNU27	9	-20°19'16.56"	-41°11'43.83"	0.0709 ± 0.020	1.136	-0.106	334.2/74.2	11.8/8.2	227.4/4.7	17.1/10.1	136.1/15.0	16.2/7.8
VNU28	9	-20°18'47.43"	-41°09'54.06"	0.0969 ± 0.016	1.212	0.304	321.2/55.4	7.5/5.5	230.9/0.2	8.9/6.7	140.7/34.6	8.7/6.1
VNU29	7	-20°18'02.78"	-41°10'15.43"	0.0541 ± 0.011	1.107	-0.551	44.4/10.8	15.9/10.4	156.7/63.4	22.3/4.5	309.5/24.1	17.01/10.4
VNU30	8	-20°16'37.93"	-41°09'33.17"	0.0480 ± 0.011	1.107	-0.214	359.3/19.6	17.9/3.7	97.2/30.6	29.6/9.3	207/68.1	22.8/13.2
VNU31	8	-20°16'23.12"	-41°09'55.50"	0.0560 ± 0.017	1.114	0.059	137.1/7.2	17.9/5.5	45.7/41.7	21.4/16.2	239.6/47.5	21.4/9.5
VNU33	7	-20°17'31.64"	-41°10'59.41"	0.0586 ± 0.022	1.280	0.376	290.9/37.1	17.7/8.1	196.8/5.5	20.0/7.5	99.6/52.3	14.1/5.9
VNU37	7	-20°17'51.43"	-41°12'59.00"	0.0616 ± 0.013	1.077	-0.546	143.9/31.9	15/9.9	315.7/57.9	39.3/10.9	51.6/3.7	39.3/10.9
Gabbros												
VNU5	8	-20°18'57.28"	-41°12'17.47"	0.1060 ± 0.020	1.436	0.185	19/48.7	6.2/4.4	285.6/3.0	11.7/4.4	193/41.1	12.7/3.0
VNU22	8	-20°18'54.75"	-41°12'19.57"	0.0931 ± 0.036	1.326	-0.260	42.1/66.4	7.6/3.1	311.0/0.5	18.3/3.3	220.8/23.6	19.3/1.4
VNU23	9	-20°17'41.43"	-41°12'27.60"	0.0015 ± 0.003	1.068	0.536	86.2/20.5	23.6/6.5	352.0/11.2	23.4/6.9	235.1/66.4	9.0/4.4
VNU24	9	-20°17'48.70"	-41°11'54.96"	0.1120 ± 0.015	1.255	0.075	53.7/20.0	18.8/3.5	311.1/30.9	19.2/5.2	171.3/51.9	7.8/4.9
VNU25	10	-20°17'14.26"	-41°11'13.54"	0.0747 ± 0.013	1.131	0.177	208.9/55.1	23.8/7.8	32.4/34.9	20.4/11.3	301.2/1.6	15.4/11.0
VNU26	9	-20°17'41.01"	-41°11'40.62"	0.0482 ± 0.013	1.118	-0.827	47.7/35.4	10.7/7.5	179.8/43.4	61.3/7.7	297.4/26.1	61.3/10.5
VNU32	10	-20°16'29.64"	-41°11'25.56"	0.0038 ± 0.001	1.071	0.205	169.5/34.9	6.6/3.0	270.0/14.7	16.5/4.6	19.1/51.3	16.4/2.9
VNU34	10	-20°16'47.32"	-41°11'25.98"	0.0866 ± 0.001	1.182	0.579	174.5/27.5	10.2/5.7	82.7/3.3	10.4/3.1	346.3/62.3	6.0/3.5
Charnockites												
VNU7	10	-20°17'15.30"	-41°13'17.74"	0.0684 ± 0.001	1.257	0.278	128.4/50.6	12.8/9.3	9.0/21.9	10.6/4.9	265.1/30.9	12.6/6.3

(continued on next page)

Table 1 (continued)

Sites	N	Geographical Coordinates		Magnetic Parameters			Main axis directions					
		Lat	Lon	K SI (mean)	P	T	K ₁ (dec/inc)	ε ₁₂ (K ₁)	K ₂ (dec/inc)	ε ₂₃ (K ₂)	K ₃ (dec/inc)	ε ₃₁ (K ₃)
VNU8	9	−20°16′36.13″	−41°12′56.96″	0.0716 ± 0.014	1.258	−0.191	143.4/55.2	8.9/6.4	19.7/21.1	14.3/7.6	278.7/26.3	13.9/6.1
VNU35	10	−20°19′18.18″	−41°12′15.18″	0.0776 ± 0.010	1.314	−0.603	39.6/56.0	10.6/6.0	271.4/22.7	13.2/6.8	170.7/23.9	13.6/9.5
VNU36	10	−20°18′25.08″	−41°13′04.51″	0.0773 ± 0.012	1.279	0.406	80.0/50.4	9.4/5.8	171.1/0.9	6.9/5.5	261.8/39.6	8.8/5.3

Note*: Site number; (N) number of measured specimens used to calculate the followed parameters; K = mean magnetic susceptibility (SI); P = anisotropy degree ($P = K_1/K_3$); T = AMS ellipsoid shape parameter ($T = 2\ln[K_2/K_3]/\ln[K_1/K_3] - 1$); K₁ = trend and plunge of magnetic lineation (in degrees); K₂ = trend and plunge of the intermediate anisotropy axis; K₃ = trend and plunge of the pole of the magnetic foliation; ε₁₂, ε₂₃, and ε₃₁ are the semiangles (measured in degrees) of confidence ellipses of AMS axes from Jelínek's (1978) statistics.

using the AGICO software ANISOFT (5.1.03) (Hrouda and Schulmann, 1990) with a minimum of five specimens. The internal dispersion is given by ε₁₂, ε₂₃, ε₃₁; sites with uncertainty >26.5° were discarded following Jelínek (1978).

The anisotropy of anhysteretic remanence magnetization (AARM) was also measured for some sites. It is a procedure that allows the extraction of the anisotropic contribution of only ferromagnetic minerals (Jackson, 1991). A total of six sites were selected according to their representability in each geological unit in the Venda Nova. The measurement of AARM was achieved through an AGICO LDA-3 demag/magnetizer and the remanent magnetization was measured with an AGICO JR6-A spinner magnetometer. The AARM was applied after alternating field demagnetization at 100 mT. Then, the AARM was acquired through 12 different orientations using a peak field value of 50 mT and a bias field of 0.10 mT. This procedure allows one to compare the magnetic fabric of all minerals given by the AMS with that of only ferromagnetic minerals provided by the AARM (Trindade et al., 2001). Deformation microstructures of the syenomonzonites and gabbro-norites were studied to infer the deformation mechanisms inside the Venda Nova. For that, oriented thin sections were made for 20 of the 37 sites of the VN (Fig. 4).

Magnetic measurements were completed with an investigation of the rock magnetic mineralogy, in at least 3 samples of each geological unit. Thermomagnetic experiments were performed on samples from the main geological facies of the VN. Samples were crushed in agate mortar and measured using a CS-2 furnace coupled to an Agico KLY-4S Kappabridge, performing both heating and cooling cycles where the magnetic susceptibility was measured against temperature. Low-temperature curves were performed after insert the sample in liquid nitrogen (ca. −195 °C) and then measuring susceptibility continually up to room temperature using the same Kappabridge instrument. High temperature curves were performed under a constant flow argon atmosphere to avoid excessive oxidation. In both high and low-temperature experiments we subtracted the signal of the sample holder and furnace. Isothermal remanent magnetization (IRM) curves, magnetic hysteresis and first order reversal curves (FORCs) were acquired for representative samples with a MicroMag 3900 vibrating sample magnetometer (VSM, Princeton Measurements Corp) to refine the magnetic mineralogy investigation.

4. Results

4.1. Microstructures

Most of the outcrops in the Venda Nova pluton lack of a distinguishable structural control, either by deformation or evidences of magmatic flow. In thin sections, sometimes preferential orientation of the fabric is present, which is mostly observable in gabbroic rocks than syenomonzonites and charnockites (once these are mostly porphyritic). Magmatic textures are preserved in most gabbroic rocks, such as the intergranular interstitial texture, in which the spaces between

plagioclases are occupied by pyroxene and biotite grains. Despite most plagioclase crystals being randomly oriented, sometimes they have marked plunging orientation (around N20°E, Fig. 4a), defining a trachytoid texture.

Submagmatic deformation is recorded throughout the whole pluton (Figs. 2 and 4), including the gabbroic core. Submagmatic flow microstructures indicate a melt-present deformation with crystal deformation, corresponding to a pre-full crystallization fabric (Blenkinsop, 2000). A crystal deformation with melt in a pre-full crystallization fabric is indicated by interstitial orthoclase in large undulating plagioclase grains and molten edges of the surrounding crystals (Fig. 4b). Evidence of a plastic deformation, such as (i) undulose extinction in quartz and (ii) discontinuous polysynthetic twins in prismatic plagioclase (Fig. 4a) where an overall igneous texture is interpreted as an indicator of sub-magmatic deformation (Vernon, 2000). Other submagmatic feature is the presence of fine-grained quartz/plagioclase occurring between large crystals of plagioclase – pointing out the presence of a melt phase under deformation during the crystallization process.

In the syenomonzonite rocks, the main magmatic feature is a porphyritic uneven texture, whose most well-developed crystals are orthoclase and plagioclase. Throughout the samples, evidence of deformation and preferential orientation is found. Magmatic features include the presence of acicular crystals (Fig. 4c), such as biotite and opaque grains. Solid-state deformation is concentrated along the border of the pluton including the charnockitic ring, besides a NE-trending “deformation corridor” that extends over the entire diameter of the pluton (Fig. 4a) that also represents evidence for solid-state deformation. Diagnostic features are: (i) aggregates of polycrystalline undulose quartz between the edges of orthoclase and plagioclase (Fig. 4d); (ii) irregular grain boundaries and strong evidence of grain boundary migration due to dynamical recrystallization (Fig. 4e); (iii) plastic deformation strips with preferred orientation (around N30°E) of quartz and biotite and secondly by opaque grains and zircon, between large feldspars (Fig. 4f, h).

The presence of a solid-state deformation corridor inside the pluton is a feature that also can be explored by studying the microstructures in a perspective of the temperature that they were formed. Deformation textures criteria – mainly of quartz and feldspars – can be applied to infer deformational thermal conditions (Passchier and Trouw, 2005). Deformation of feldspar probably occurred in low-medium grade conditions (between 400 and 500 °C) where deformation still occurs mainly by internal microfracturing, however, enhanced by minor dislocation glides, as evidenced by textures as (Passchier and Trouw, 2005): (i) border migration by bulging (BLG) recrystallization of orthoclase (Fig. 4g), characterized by the local boundary mobility of grains forming a mineral peninsula (Prior, 1993), (ii) undulose extinction of feldspars and (iii) bent twins of plagioclase (Fig. 4g). Quartz in such corridor forms aggregates of new grains (Fig. 4h). Recrystallization diagnostically generates strain free grains (in the aggregates) that are capable of continued deformation (Vernon, 2018). The syenomonzonites composing this zone seems to show partition deformation in portions



Fig. 3. Fieldwork scenarios from the Venda Nova pluton. Planes demonstrated in the upper corner of the stereograms represent the direction of the metamorphic foliation at the country rocks. a) Dextral kinematics from a dynamic deformation in granitic and syenitic dikes intruding the western charnockitic ring. b) Isoclinal folds showing west vergence in the SW border of the Venda Nova pluton, in c) deformation of the orthogneiss with lots of ductile deformation evidence in the NE border and d) quartz boudinage with vertical milonitic foliation in the NW border— the three highlight plastic and dynamic deformation around the elliptical intrusion of the syenomonzonite envelope of the pluton. e) to g), represent some features inside the Venda Nova. e) shows a clear abrupt contact between syenomonzonites and the gabbroic core, more easily observed in the core sampled (f) at the limits represented by the yellow dots in (e). In (g) a gabbroic dike cuts the NW syenomonzonitic border, with major evidence of physical and little mixing interaction. (For interpretation of the references to colour in this figure legend, the reader is referred to the Web version of this article.)

rich in weak minerals, (i.e. biotite and quartz between porphyritic feldspars), forming fine aggregates characteristically of high strain local zones surrounded by less deformed large grains (Fitz Gerald and Stünitz, 1993; Shea and Kronenberg, 1993; Goodwin and Tikoff, 2002). Grain size reduction in coarse-grained rocks are associated to the development of foliation/lineation, which are associated with the weaker aggregates (Vernon et al., 1983).

In the Venda Nova pluton, there is a hiatus between solid-state deformation (restricted) and submagmatic deformation (spread in the entire intrusive body), suggested by the absence of higher temperature

solid-state macrostructures. Furthermore, the deformation corridor in the Venda Nova pluton matches with NE-SW direction of regional shear zones, as the GSZ, and with a lineament that sections VN throughout the whole corridor.

4.2. Magnetic mineralogy

Thermomagnetic (K–T) curves of samples from each studied unit show signatures of minerals with ferromagnetic behavior (Fig. 5). The spontaneous warming of the samples after their insertion on liquid

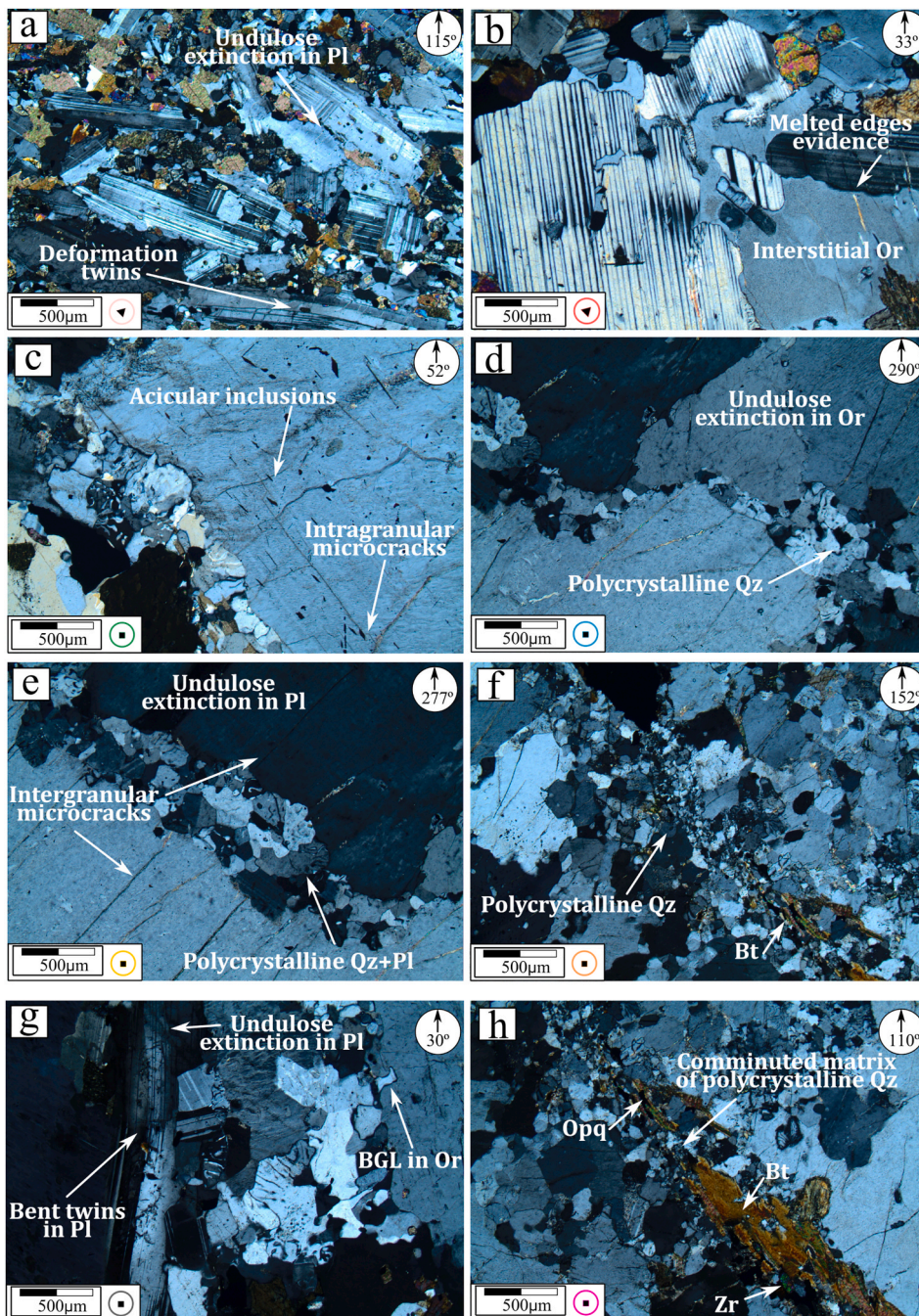


Fig. 4. Micropetrographic thin sections of Venda Nova pluton samples. Colored symbols at each thin section matches the sites of Fig. 2. Sections were oriented according to the core azimuthal orientations in the field (indicated at the upper right corner). In a) deformation twins in plagioclase and undulose extinction in plagioclase, b) shows interstitial orthoclase in plagioclase, both in gabbros. c) shows acicular inclusions, sometimes filling intragranular microcracks in syenomonzonites. From (d) to (h), polycrystalline quartz strips together with undulose extinction in orthoclase and quartz are evidence of sub-solidus state deformation in syenomonzonites. In the “deformation corridor” there is evidence of deformation in temperatures around 400–500 °C, such as BGL in orthoclase and bent twins in plagioclase.

nitrogen indicated an abrupt increase of susceptibility for all samples that begins around -180 °C to stabilize about -150 °C. This behavior is assigned to the Verwey Transition of magnetite (VT), although the slight differences of the VT in each sample might be an expression of a non-stoichiometric or the oxygen deficiency of its chemical composition (Dunlop and Özdemir, 1997). In high temperatures, all samples show a sudden fall of the magnetic susceptibility at 580 °C, which is the Curie temperature of magnetite (MCT), manifesting the dominance of this mineral over the whole magnetic fabric. For the charnockitic and gabbroic samples (Fig. 5b', 5c') there is an increase of the magnetic susceptibility before the MCT, possibly related to the Hopkinson Effect. The heating and cooling K-T curves for the syenomonzonitic rocks show reversibility (Fig. 5a'), meaning that no ferromagnetic mineral transformation occurred during the process. While this last curve exhibited paramagnetic behavior soon after MCT, the curves of charnockitic and

gabbroic rocks kept a sluggish decay, trespassing the Néel temperature of hematite (680 °C), which is an indication of its presence. Also, the cooling curves for these samples show increase of (K), pointing out the probable formation of new ferromagnetic phase. Distinguishing paramagnetic and ferromagnetic contributions to the thermomagnetic curves through the semi-quantitative hyperbole of Hrouda et al. (1997) pointed that less than 1% of the measured susceptibility correspond to paramagnetic phases among the three studied units.

We plot raw and corrected (excluding dia/paramagnetic) hysteresis of three sites in Fig. 6. The slope of acquired magnetization at high fields shows that paramagnetic contribution to the magnetic fabric of most samples correspond to less than 1% (similar to the answer of thermomagnetic curves), once raw and corrected hysteresis are quite similar. Gabbros from the site 32, however, show a distinct behavior: the angular coefficient at high fields is comparable to the slope at low fields, possibly

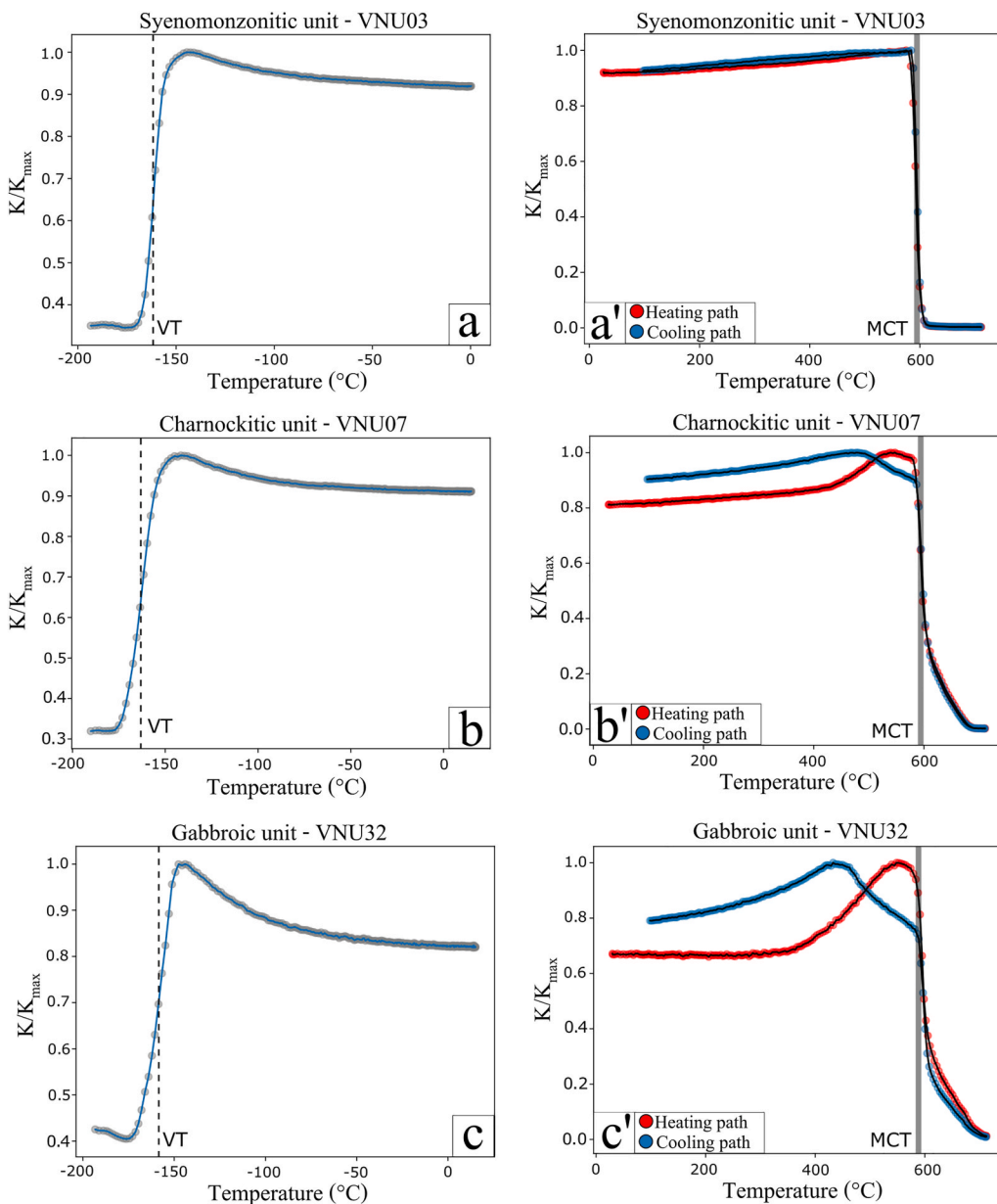


Fig. 5. Thermomagnetic curves for the main units of the VN, normalized by the maximum magnetic susceptibility of each sample. The left side graphics show curves for cryogenic temperatures (a,b,c), all of them characterized by the Verwey Transition (VT). The vertical dashed line indicates the VT around -153 °C. High temperature curves are on the right side graphic column (a',b',c'). Charnokitic and gabbroic samples showed, besides magnetite, the presence of another ferromagnetic mineral – probably hematite, due the paramagnetic behavior tendency only observed after 680 °C, which is the Néel temperature for hematite. The gray vertical bar indicates the magnetite Curie temperature around 580 °C.

indicating a greater paramagnetic contribution.

The magnetic hysteresis curves highlighted normally low coercivity values (H_c) (in a range of 18.75 – 0.932 mT). The hysteresis loops for most of the samples have a thin waist – indicating that the low H_c values are probably associated to multidomain (MD) magnetite. The VNU32 sample exceptionally shows a characteristic “wasp-waisted” loop (Fig. 6c), which indicates the presence of two magnetic minerals (Tauxe et al., 1996). As suggested by the thermomagnetic curves, (see above) these minerals are probably magnetite and hematite, which must make part of the rock magnetic fabric. Compared with other lithologies, the gabbro shows low values of IRM (Fig. 6d), which does not reach saturation at fields of $0.8T$. Added to its high H_c , this is another evidence of the presence of hematite in this rock. The coercivity of remanence (H_{cr}) is similar for all samples, including the gabbros, with the exception of that from site 32. The Mrs/M_s (in a range of 1.46×10^{-2} – 0.0298×10^{-1}) and H_{cr}/H_c (in a range of 5.62 – 30.60) ratios are typical of those found for MD magnetite, according to the Dayplot diagram (Fig. 6e) (Day et al., 1977), with exception for VNU32 sample, which falls into the pseudo-single-domain (PSD) field. FORC diagrams (Fig. 6) performed

for some samples corroborate the previous interpretation that MD magnetite particles predominated in the studied samples due to the vertical spreading along the interaction (B_u) axis and a lesser contribution parallel to the coercivity axis (B_c), behavior that characterizes the MD structure (Pike et al., 2001). Such results demonstrate that, even if other magnetic carriers are present in the VN, MD magnetite must be the predominant.

Temporim et al. (2021) have used paleomagnetic data of Venda Nova and Santa Angélica (SA, Fig. 1c) plutons (another southern post-orogenic pluton 40 km near Venda Nova, see Fig. 1c) to establish a key-pole to Western Gondwana in the Cambrian that accomplished all reliability criteria of both Van der Voo (1990) & Meert et al. (2020). The authors showed that although the majority of VN magnetic particles are indeed MD magnetite – which carry viscous magnetization (VM) – most samples have a small contribution of high coercivity and high blocking temperatures with stable thermoremanent magnetization (TRM). We measured the natural remanent magnetization (NRM) of Venda Nova rocks inside a blinded shield room with a JR6 spinner magnetometer (AGICO). NRM intensities values are above 0.1 Am^{-1} (Supplementary

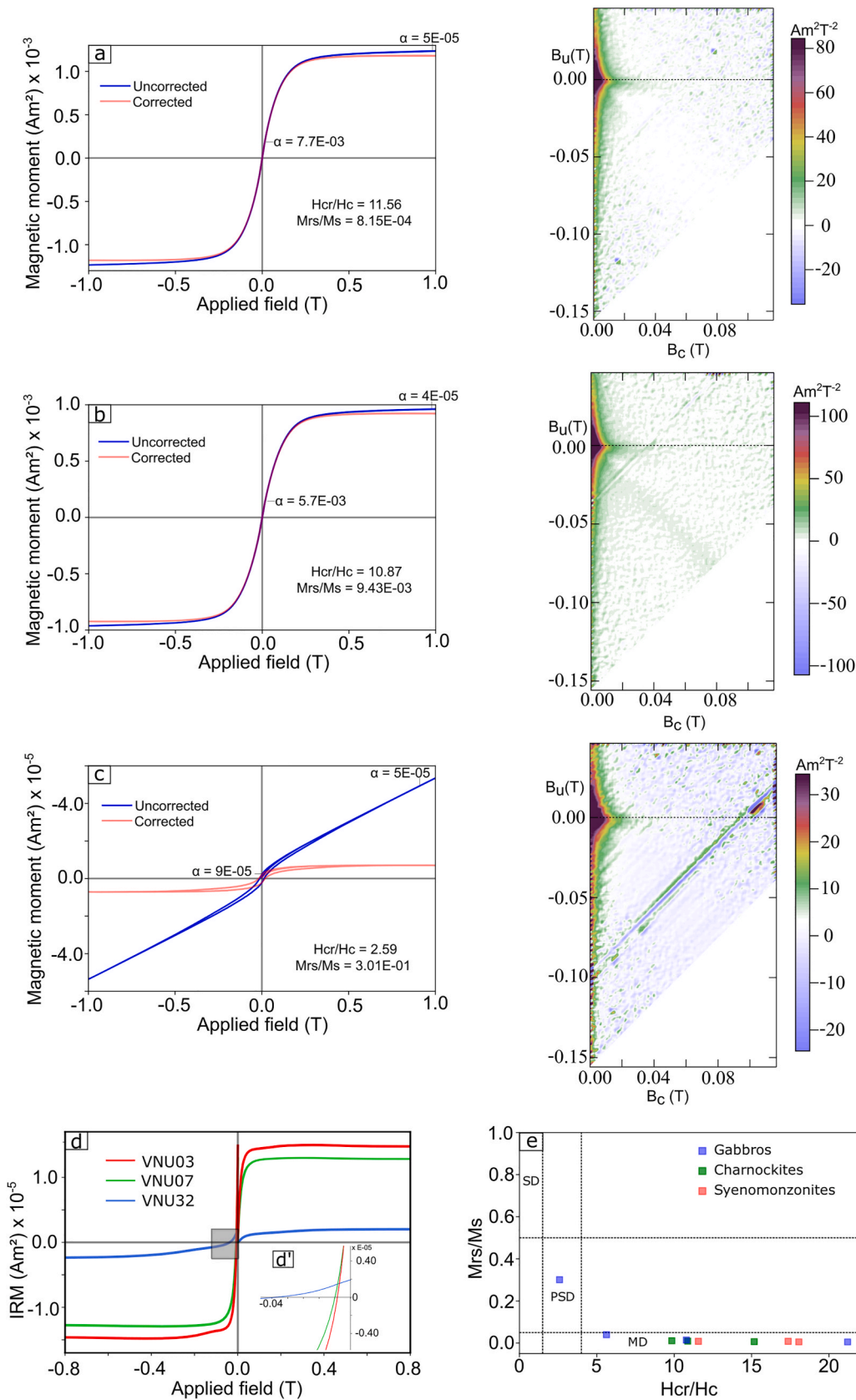


Fig. 6. Magnetic Hysteresis, FORC diagrams and IRM for representative samples from the units of the Venda Nova pluton: a) VNU03 (syenomonzonite), b) VNU07 (charnockite) and c) VNU32 (gabbro). d) Shows the IRM acquisition in the positive and negative induced field, d') is a zoom in the grayish frame showing the H_{cr} defined when the curve crosses the abscissa axis and e) shows the Day diagram for specimens of the Venda units. The hysteresis slope of low and high fields are pointed by α .

file) (Fig. 7a). Plotting sites mean NRM directions using Fisher (1953) statistics results in a really high dispersion (Fig. 7b). NRMs are usually a vector sum of stable/unstable magnetizations (Butler, 1992; Tauxe, 2005). In the Venda Nova rocks, NRM is a result of VM (MD magnetite) + TRM (SD/PSD magnetite) (Temporim et al., 2021), the dispersion observed in our measurements is another indication of MD magnetite (once it composes most of the NRM spectra).

4.3. Anisotropy of magnetic susceptibility (AMS) and anisotropy of anhysteretic remanent magnetization (AARM)

Table 1 summarizes the results of the site mean principal susceptibility axis (K_1 , K_2 and K_3) parameters and their associated errors, and site mean parameters K , P and T of the measured AMS. Besides the criteria established by Jelínek (1978), the quality magnetic data from each specimen was tested following Pueyo et al. (2004). The ϵ_{31}

confidence angle of all measured specimens are below 10° , while the corrected anisotropy degree is greater than 1.02, which attests high accuracy of the measured anisotropy (Fig. 7c). With exception of two specimens of the syenomonzonites and a single one from the gabbroic core, ϵ_{12} is smaller than 20° for all of the other ones – confirming that magnetic lineation is reliable (Fig. 7d). Magnetic foliation also shows high credibility, since only 3 specimens of the syenomonzonites and a single gabbroic one are above have ϵ_{23} above the reliability cutoff (20°) (Fig. 7e).

The bulk magnetic susceptibility of specimens (k) varies widely in the VN (Fig. 7f). The smallest values are concentrated in the middle-NW of VN, mostly in syenites and monzonites and throughout the charnockitic rocks in the extreme NW portion (Fig. 8a). The highest values are distributed in the southern portion of the VN, related to the southern part of the gabbroic core. For the syenomonzonitic unit, the arithmetic mean susceptibility and standard deviation are $7.25 \times 10^{-2} \pm 2.75 \times$

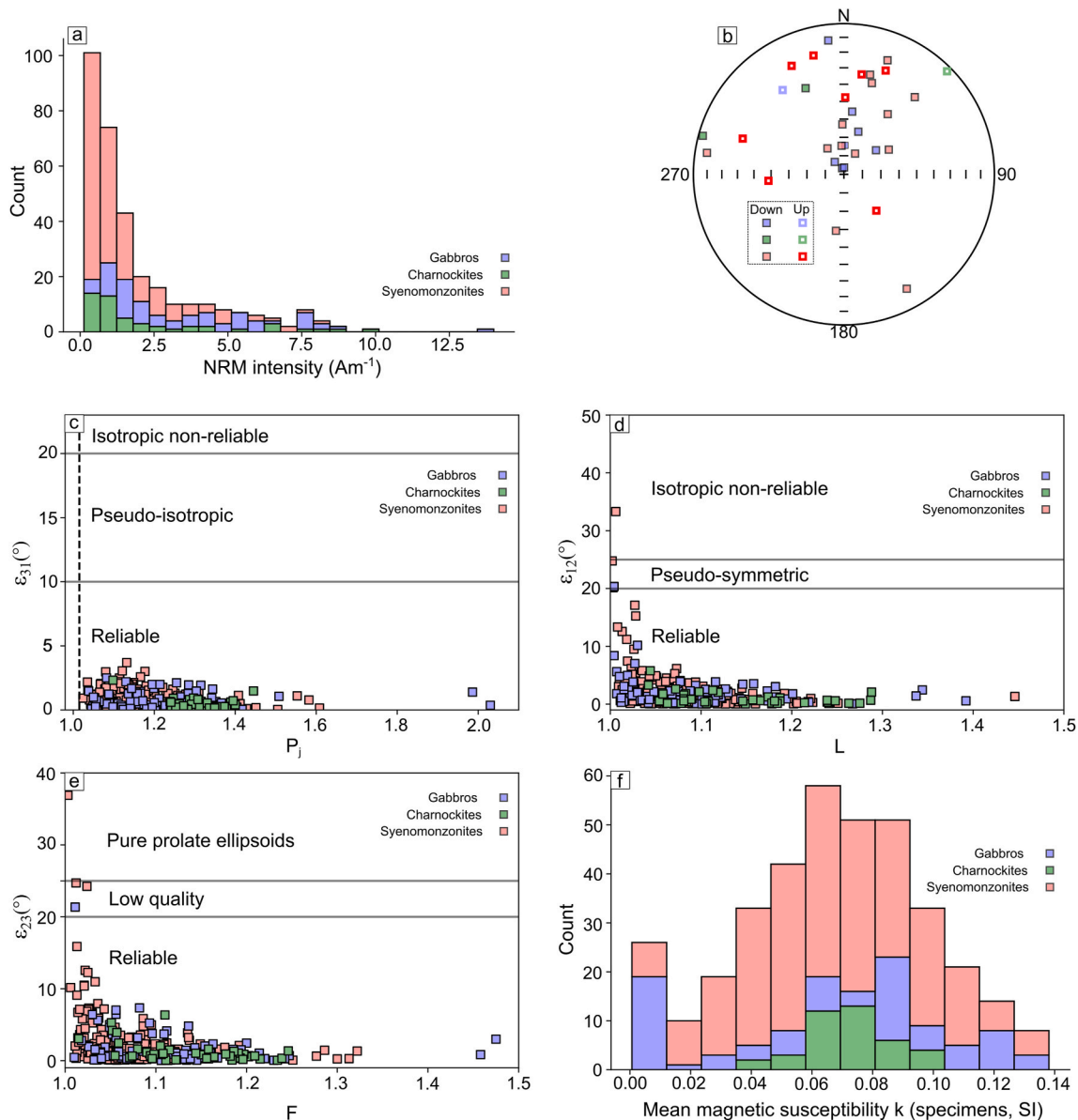


Fig. 7. a) natural remanent magnetization (NRM) histograms of intensity and (b) dispersion on Schmidt-net (mean directions per site, following Fisherian statistics) (specimens). The lack of grouping in NRM directions is interpreted as result of the viscous remanent magnetization carried by MD grains of magnetite. c) ϵ_{31} vs P_j plot indicates the highly accurate anisotropic data, where $P_j = \exp\sqrt{2[(\ln k_1 - \mu m)^2 + (\ln k_2 - \mu m)^2 + (\ln k_3 - \mu m)^2]}$ and $\mu m = [(\ln k_1 + \ln k_2 + \ln k_3) / 3]$. d) ϵ_{12} vs L plot shows that magnetic lineation is reliable, where $L = (k_1 / k_2)$. e) Degree of magnetic foliation (F) has ϵ_{23} values majorly $< 20^\circ$ assuring its reliability, where $F = (k_2 / k_3)$. f) histograms showing magnetic susceptibility (specimens) hued by the main lithotypes of VN.

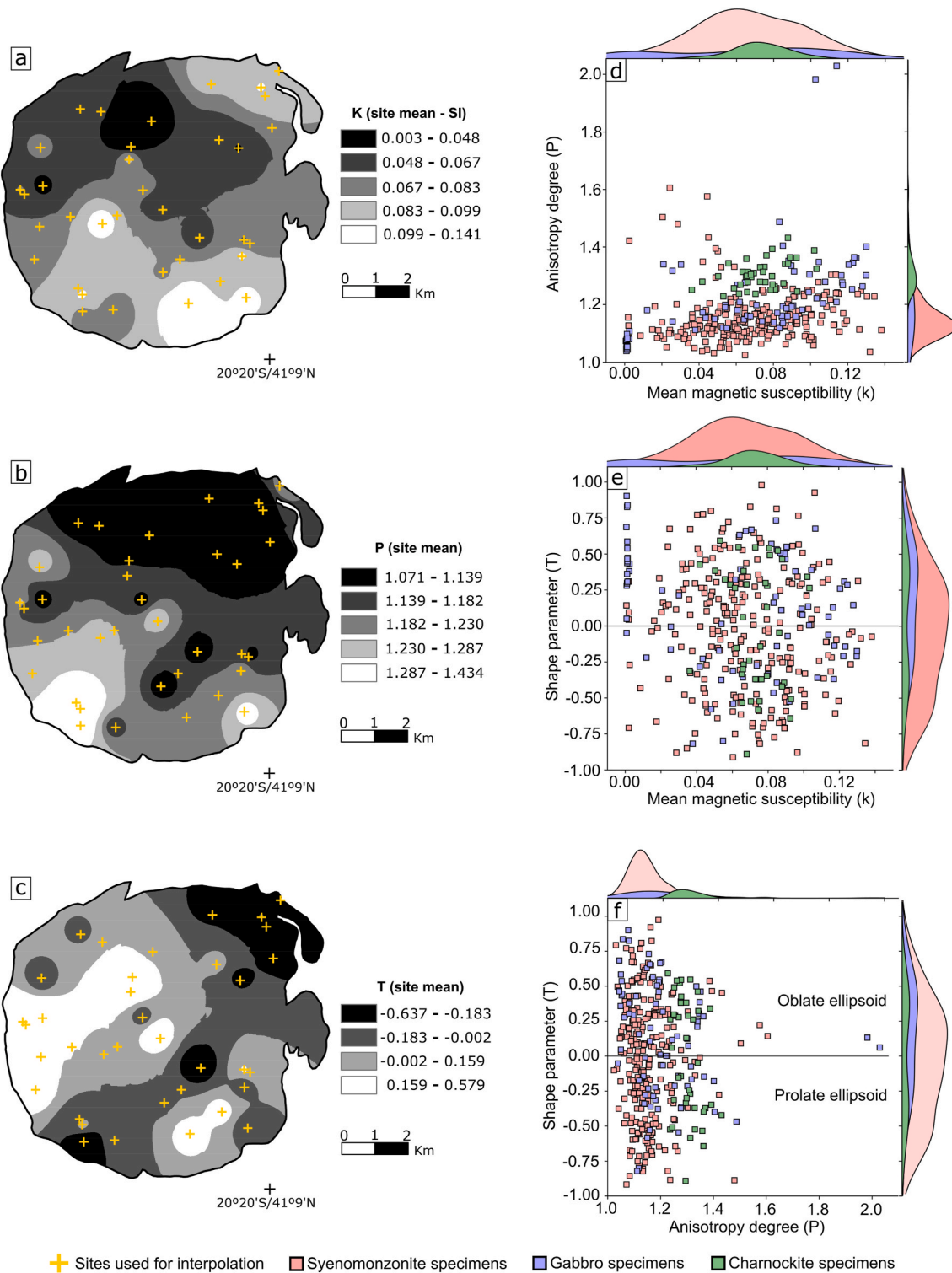


Fig. 8. Scalar magnetic parameters calculated through AMS data. Interpolation through minimum curvature of bulk magnetic susceptibility (K) (a), anisotropy degree (b) and shape parameters (T) throughout the pluton. d) P vs k, showing a wide spread of susceptibilities. e) T vs k showing a wide variability of the data, with no predominance of shape anisotropy, oblate or prolate, and no visible relation of T with susceptibility (K). f) Jelinek plot (T vs P), also demonstrating almost equal distribution between oblate and prolate ellipsoids.

10^{-2} , which is similar to those calculated for gabbroic rocks with $6.51 \times 10^{-2} \pm 4.06 \times 10^{-2}$. This variability is not repeated for charnockitic rocks, whose average susceptibility value is $7.37 \times 10^{-2} \pm 0.45 \times 10^{-2}$, indicating a standard deviation with an order of magnitude lower than those obtained for the other lithologies. This analysis of spatial variability of K determines that there is no relationship between a lithotype

with a high or low value of K (Fig. 8a). The average site mean anisotropy degree (P) varies from 1.071 (VNU32) to 1.434 (VNU5) (Fig. 8b). The “P” values cannot be directly related to the pluton units as well, since they are variably dispersed throughout the area (Fig. 8b). However, the lowest values are in the northern portion of the body, indicating a low “ $K_1 * K_3^{-1}$ ” ratio.

The shape of the ellipsoids (T) varies widely, from -0.637 to 0.579 (Fig. 8c). This figure shows a NE-SW direction strip of prolate ellipsoids in the east side of the VN that matches with the less anisotropic portion in the same region, as shown in Fig. 8b. The range of the highest T values is mostly concentrated in the northernmost part of the pluton, indicating ellipsoids with the highest oblate shapes, which are also associated with the less anisotropic rocks (see Fig. 8b). On the other hand, areas where predominate oblate ellipsoids ($T > 0$) are mostly associated to the highest anisotropy degrees ($1.434 > P > 1.287$) (compare Fig. 7b and c). These bands with prolate and oblate ellipsoid shapes cannot be explained as a specific feature associated to any unit within the pluton. Fig. 9 shows the AMS and AARM results for six sampling sites, distributed in all lithotypes of the VN. The AMS and AARM magnetic fabrics are very similar for all lithotypes, thus attesting the dominant role of the MD magnetite in the definition of the rock magnetic fabric. Any other magnetic phases, even if present in the samples, seem to have minimal influence in the AMS of the studied rocks.

5. Discussion

5.1. Significance of magnetic fabric

Multidomain (MD) magnetite was identified as the main carrier of the anisotropy of magnetic susceptibility in the VN. Magnetic fabric carried by such mineral component with coarser-grain dimensions has been interpreted as coherent with magmatic flow and magmatic foliation (Archanjo and Bouchez, 1997; Archanjo et al., 2008; Payacán et al., 2014). Although hematite is also detected in some rock units, the thermomagnetic curves and magnetic hysteresis, supported by FORC diagrams, as well as the AARM ellipsoids acquired from the induced magnetization of a peak field value of 50 mT (i.e., we restrained the coercivity range to receive only AARM data of the largest magnetic carriers) confirm that MD magnetite controls the magnetic fabric. The presence of MD magnetite is extremely important for AMS studies, once it is controlled by magnetostatic energy (shape anisotropy) instead of the magnetocrystalline anisotropy (Dunlop and Özdemir, 1997).

Correspondence between the orientation of rock fabric and magnetic fabric are supported when comparing AMS eigenvectors (i.e. magnetic lineation plunging and magnetic foliation strike) with preferential orientation of larger feldspathic grains and deformation strips in the thin sections (as reported in 4.1).

The highest values of anisotropy degree P (up to 1.43) in the SE/SW sector of the Venda Nova pluton match the description of dynamical deformation (Mendes and De Campos, 2012) and the solid-state deformation found in the thin sections. This observation coincides with the distribution of oblate ellipsoids, according to the T values (Fig. 8c), extending from the charnockites to the gabbroic core. Once the P parameter measures the relation between the largest and the lowest eigenvalues and, consequently, in an oblate fabric – the observation between high and intermediary values of P in this portion can be both related to solid-state deformation as for sub-magmatic deformation. The magnetic lineation is predominantly concentric, pointing to the center of the pluton (Fig. 10). The borders exhibit high plunging angle ($60\text{--}90^\circ$) interpreted as a result of border deformation due a vertical emplacement of the magmas. K_1 inclination values range from 0 to 30° in the most centered part of the VN, including the gabbroic core. K_1 in the syenomonzonitic envelope point out that buoyance forces acted dragging the flow inwards. The magnetic lineation inside the gabbroic core has low plunging angle, indicating a distinct magmatic feeding when compared with the syenomonzonitic rocks. This observation is also supported by the geographic position of the gabbroic core, shifted to the west and near the charnockitic border – which would cause an increasing plunging angle near the western border of the core – instead of the measured subhorizontal lineation. Magnetic foliation supports the rounded concentric pattern (Fig. 10) which agrees with the magmatic foliation recorded in the pluton (Mendes and De Campos, 2012).

The strong fabrics created by solid-state deformation correspond to high values of P (up to 1.43) and an oblate fabric, observed through the values of T, extending from the charnockites to the gabbroic core (Fig. 8). Microstructural analysis and AMS data confirms the predominance of solid-state deformation features along a NE-SW deformation corridor that transects the pluton. Magnetic foliation in this sector (perpendicular plane to K_3) assumes strikes of NE-SW directions with dip angles above 60° . Magnetic lineation (K_1) has low-to-sub-horizontal plunges, with trends parallel to the magnetic foliation strike. Contrasting with the general concentric pattern in the whole pluton, these features seem to be related to low-medium grade conditions that we interpreted as distinguished from the submagmatic features. Magnetic lineation also matches the direction of acicular inclusions and oriented biotite in samples from sites of such profile of the VN (Fig. 4f), together with polycrystalline aggregates of quartz and opaque minerals (Fig. 4h). This observation is also very relevant, because location fabrics of magnetite inclusions commonly occurs parallel to mafic silicates, especially micas (Borradaile and Henry, 1997). AMS may record strain and track paleostress, once correlations of the ellipsoid formed by the eigenvectors are parallel to the deformation ellipsoid, i.e., K_1 is parallel to the stretching lineation (X-axis) and K_3 is parallel to Z-axis (perpendicular to the XY plane) (Borradaile and Henry, 1997). Therefore, we interpreted that AMS data indeed agrees with the existence of a deformational zone inside the pluton, coherent with the regional dextral transpressional shear zones and anticline hinges (Alkmim et al., 2006) that controls the regional trend of the pre-to-syn-orogenic units near the Venda Nova, such as the GSZ.

5.2. Emplacement of Venda Nova pluton

The deflection of foliation in the country rocks that envelops the pluton in high deep angles and structures of dynamic deformation (see section 2.3), is an important indication of the emplacement mechanism of the VN. The passive magma transport related to diapiric and plutonic features occurs through ductile or brittle faults and shear zones (Nédélec and Bouchez, 2015). These deep structures might work as easy escapes to fluids to rise through the crust (Rosenberg, 2004; Weinberg et al., 2004; Cavalcante et al., 2016; Seymour et al., 2020) and have been interpreted as channel structures for post-orogenic plutons in the AO (Wiedemann et al., 2002; Pedrosa-soares et al., 2007). Similarly, the diapiric mechanism has already been summoned by Bayer et al. (1987) to explain the emplacement of the Santa Angélica pluton. As the diapir ascends through the crust, it accumulates in a spherical chamber and deforms the surrounding rocks, causing a ductile downward flow of the country rocks that is printed as foliations of high angle dips (Bridgwater et al., 1974; Paterson and Fowler, 1993) enveloping the VN pluton. This observation is clear in the pre-to-syn-orogenic units of the VN, which return to the regional (NE-SW) trend a few kilometers away from the contact with the pluton.

Although interpreted as a single plutonic feature, units of the Venda Nova seems not to have intruded as a single act. Concentric zoning (Fig. 10a), such as in the VN, has been interpreted as a typical feature of post-orogenic plutonism resulting from differentiation and/or contamination processes (Holder, 1979). The existence of inversely zoned pluton is possible due a relationship between magma composition, temperature and, therefore, viscosity. When magmas of different temperatures come in contact, thermal equilibrium is quickly achieved, followed by a constant cooling rate, but each magma flows at its own viscosity, ensuring that complete hybridization only occurs if the initial composition of both is very similar (Nédélec and Bouchez, 2015). Different units inside the same pluton are hardly considered to be emplaced as one single act (Harry and Richey, 1963).

The idea that charnockite and norite units of the VN could not be derived from the same parental magma that crystallized the inner gabbroic core was indorsed by mineral chemistry (Mendes and De Campos, 2012). In fact, norites and charnockites themselves show

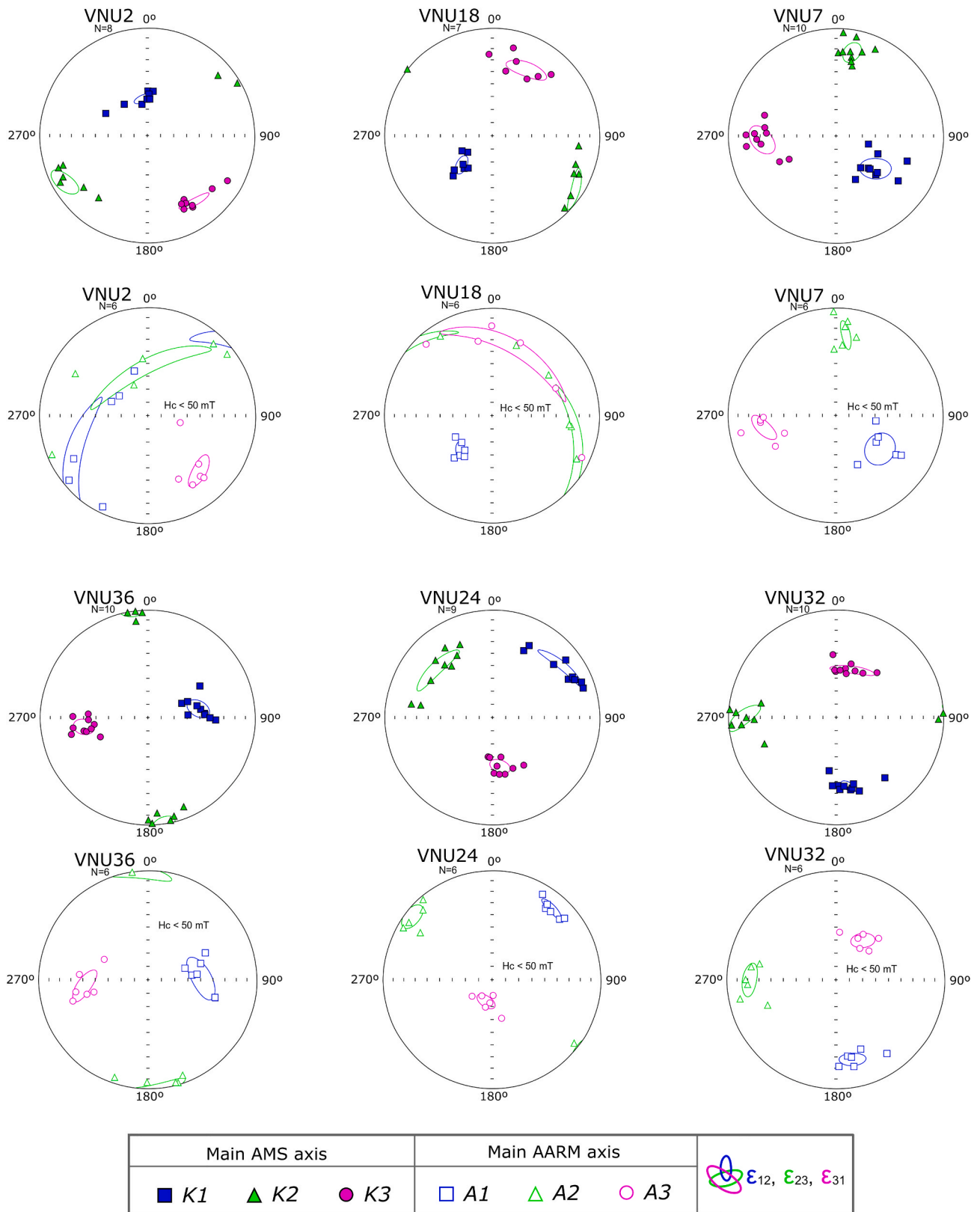


Fig. 9. Direct comparison between AMS and AARM for synmonzonitic samples (VNU2, VNU18), charnockitic (VNU7, VNU18) and gabbroic (VNU24, VNU32) samples. The AMS is an answer of diamagnetic, paramagnetic and ferromagnetic minerals, while AARM represents the contribution of only ferromagnetic minerals. The coincidence between the main susceptibility axis of the AMS and AARM ellipsoids implies that magnetic fabric of the Venda Nova pluton is controlled by the MD magnetites as suggested by magnetic mineralogy.

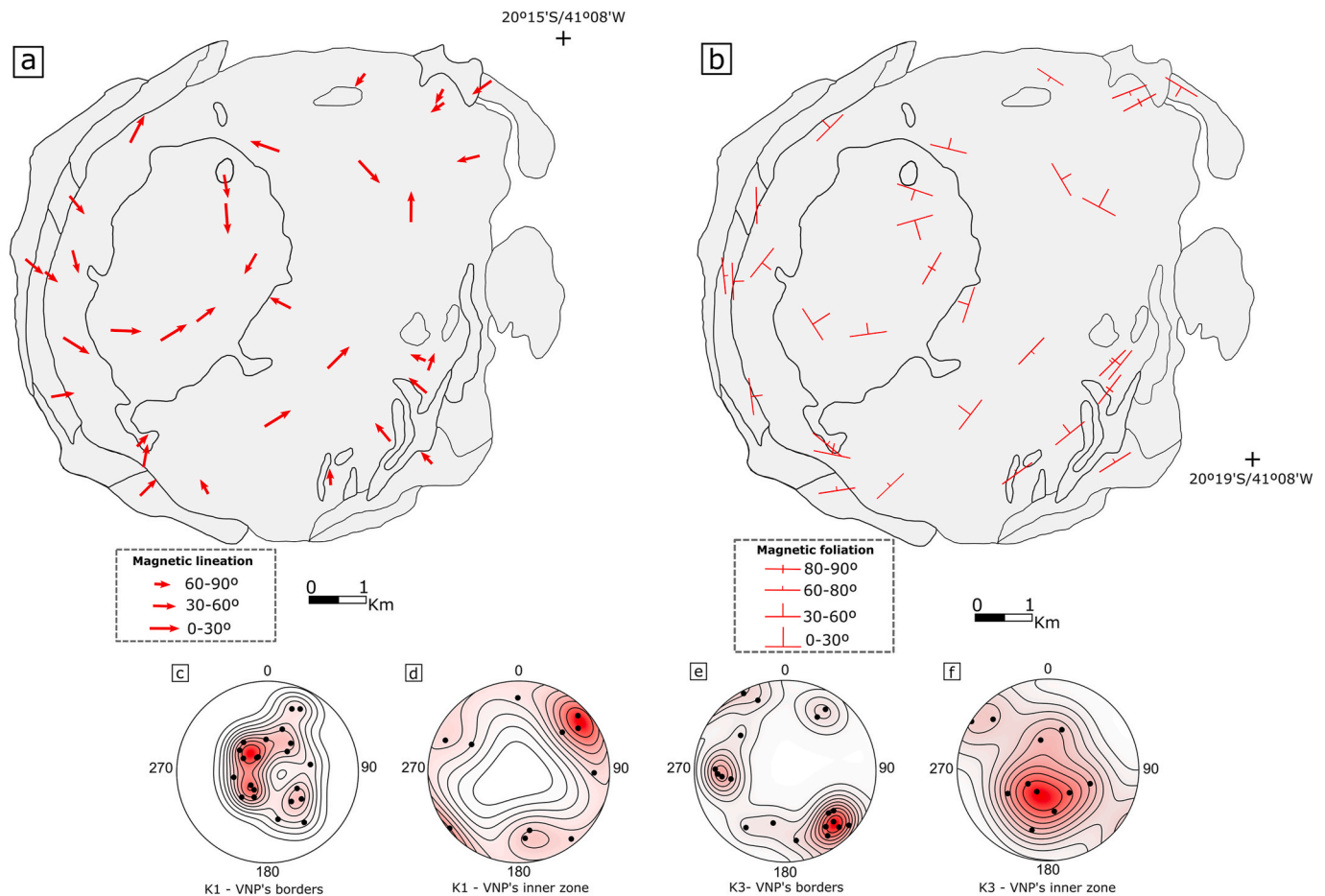


Fig. 10. Map of AMS directional data after filtered by the [Jelinek \(1978\)](#) dispersion criteria. a) Magnetic lineation (K_1) and b) magnetic foliation (orthogonal plane to K_3) both showing a concentric pattern for the whole intrusion. Plunging of magnetic lineation at the borders (c) and inner zone (d) (which includes the gabbroic core) show high angles and lower angles, respectively. Same approach is considered for the magnetic foliation, with more horizontal poles concentrated at the borders (e) and, mostly vertical poles for the inner zone (f).

different chemical signatures, tholeiitic and calc-alkaline, respectively. Magnetic foliation of the charnockites have high dip angles that points to the inner part of the pluton. Although this a recurrent aspect of the fabric at the borders of the syenomonzonites as well, charnockitic rocks have high anisotropy degrees and macroscopic evidence of solid-state dynamic deformation (granitic and syenitic dikes) that reflects an oblate fabric. These evidences suggest, in fact, that VN outer ring (charnockitic) is a previous structure that should have intruded the crust earlier than the syenomonzonite and gabbroic units, and later deformed by its ascension. Such deformation works in the same perspective as the observed in the country rocks, through a downfolding mechanism.

Compared to other units in the VN, the gabbroic core represents a topographic low, pointing out the intensity of the weathering processes that have limited the amount of exposed outcrops. [Ludka et al. \(1998\)](#) described the contact between the facies of the pluton as gradational features, suggesting coeval intrusion of these magmas with their felsic neighbors, although these features were not observed in our field work. However, field evidence also shows abrupt contacts between the southernmost portion of the gabbroic core with the syenomonzonitic envelope ([Fig. 3d](#) and e), whereas large idiomorphic grains of alkali-feldspar migrates from the felsic rocks to the near gabbroic unit – evidencing chemical disequilibrium and corona textures ([Ludka et al., 1998](#)). A most-liquid hot basic magma could have host a large feldspar grain migration from a semi-solidus felsic magma. This would mean that, although nearly contemporaneous in the whole intrusion scenario, the syenomonzonitic unit could have been an earlier pulse (compared to the gabbroic core).

Submagmatic deformations inside the gabbroic core show that more felsic material might have been slowly injected to the system, which is reinforced by the observation of well-crystallized grains with melting evidence on its borders. In this case, submagmatic flow was probably caused by the arrival of new pulses of magma in the magma chamber. Mafic dikes cutting the syenomonzonites in the northernmost part of the VN are ductile deformed and show mingling interaction. To support such observation - consider the hottest section of VN being the west due the presence of the gabbroic core - the syenomonzonites must have been relatively solid for the intrusion process, but molten enough so the mingling and ductile features would occur. Besides, samples from the syenomonzonite near the contact with the gabbroic core shows that magnetic lineation and foliation plunges inwards the core ([Fig. 10b](#)). Furthermore, magnetic foliation inside the gabbroic core seems to impart its own concentricity, indicating that magmatic flow accumulated in a specific region inside the pluton, forming the core.

Some papers have already approached the origin of magmas in the Venda Nova: syenomonzonitic magma has a shoshonitic chemical signature and high Ba, Sr and LREE values (e.g. [Ludka et al., 1998](#)). Gabbroic rocks are basaltic to high-K-basaltic suits but, also, show relative enrichment in those elements ([Horn and Weber-Diefenbach, 1987](#); [Ludka et al., 1998](#)) and are interpreted as coming from a previously contaminated mantle source.

As described by [Wiedemann et al. \(2002\)](#) and references therein, during the 530-480 Ma period, ductile stretching through the AO, together with discordant dikes, suggest a change to an extensive regime. [De Campos et al. \(2016\)](#) also stated that the intrusion of coeval plutons

around 500 Ma in a corridor from south to north AO must have a common tectonic trigger – such as a crustal relaxation zone that is parallel to the AO metamorphic core happening shortly after orogenic collapse – becoming a path from basic magmas (such as the VN gabbroic core) that originates from partial decompression melting of an asthenospheric mantle. For the units of the VN, we propose that an upwelling of the asthenospheric mantle may have caused tensional stress at the Moho, also providing heat to the surrounding crust.

Through rheological deep weak structures, trapped charnockitic and noritic magmas would intrude the mid-lower crust levels (as indicated by geobarometric data of the VN charnockites, Mendes and De Campos, 2012) ascending as diapir like structures (Fig. 11a). Later on, syenomonzonitic magma would follow the same path to intrude the first charnockitic pulse, deforming it and causing solid-state deformation found throughout such unit (Fig. 11b). Once temperature is an important crustal viscosity factor control (Gerya and Burg, 2007) and melts provide faster emplacement – a hotter crustal contaminated basaltic

magma enhances the upward movement of alkaline melts. Alkaline and basic magma intruding and ascending together could therefore have physico-chemical conditions to form the hybrid rocks reported by Ludka et al. (1998). The gabbroic core emplaces itself through a partially crystallized syenomonzonitic envelope (Fig. 11c). As the basic magma ascends, paraderived country rocks suffer melts (Ludka et al., 1998) at the borders of the channel structure and allow the emplacement of granitic bodies at the border of the alkaline-magma unit.

The major concentric pattern of the magnetic fabric in the syenomonzonites and gabbros of the Venda Nova indicates that buoyance forces were prevalent in most of the emplacement of the Venda Nova. Similar interpretation for the driven forces that controlled the intrusion of southern plutonic features in the Araçuaí was given by Temporim et al. (2020b), once a concentric fabric mostly indicates that little or no tectonic influence in the emplacement of these magmas (Sant’Ovaia et al., 2000; de Oliveira et al., 2010). However, a deformational corridor inside the Venda Nova pluton conflicts this general pattern. In the

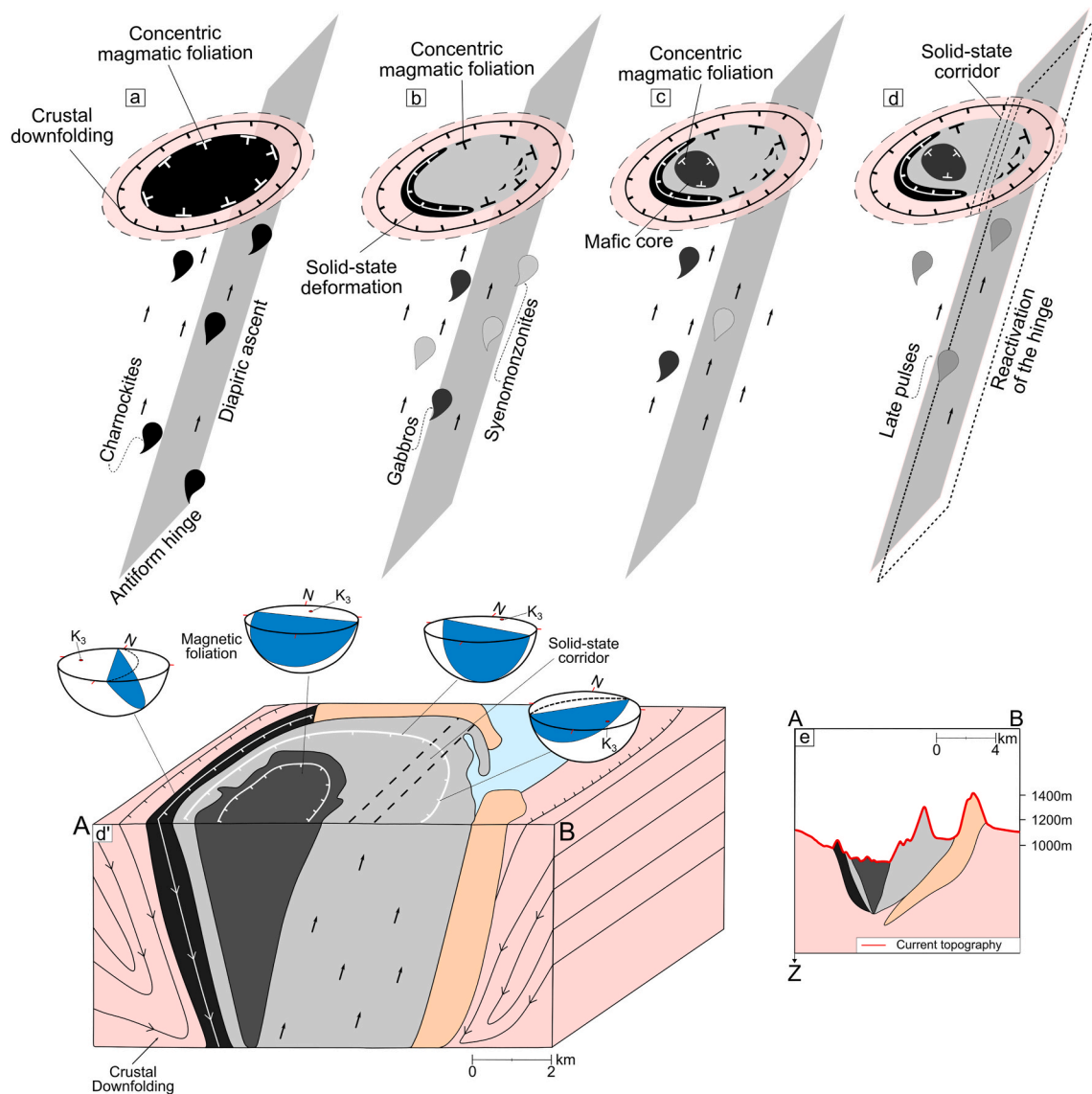


Fig. 11. a) to d) represents the emplacement of the Venda Nova and the structures formed in each step. For sake of clarity, the norite and charnockite from the west border were represented as a single unit. In d') it is provided a structural scenario of the last stage of the Venda Nova pluton emplacement (d), based on the AMS and micropetrographic data. Semi-spheres shows the magnetic foliation of a few sites of the VN, evidencing the general concentricity in the syenomonzonitic envelope and gabbroic core. Black arrows indicate the ascension of the magma flow that causes a reactivation of the weak structure, for which the VN could have intruded, in the last stages of its crystallization. Downward folding of the country rocks (reverse arrows) and the external charnockitic ring reflects the concentric metamorphic foliation and AMS data, respectively. e) Profile showing the current topography (A–B).

Canadian shield, post-tectonic granitoids show general concentric magmatic fabrics, but a cryptic tectonic fabric parallel to the external schistosity of the country rocks, recorded by MD-magnetite, which acted as a recorder of regional tectonic stress after the intrusions froze (Borradale and Kehlenbeck, 1996). This corridor in the VN concentrates solid-state deformation of mid-low temperatures, indicating that Venda Nova rocks should have suffered some stress in during the last stages of its crystallization. The fabric orientation in such corridor matches the directions of the regional NE-SW trend in the southern AO as well as a structure indicated by Wiedemann et al. (2002) as an anticline axis.

5.3. Implications for the post-orogenic magmatism in the Araçuaí orogen

The concentric fabric of VN and its inner sub-magmatic deformations confirm its post-orogenic nature as previously suggested by geochemical data (Mendes and De Campos, 2012; De Campos et al., 2016) and elucidates that little, or no significant influence of tectonic strain acted during most of its emplacement. However, in the last stages of its crystallization it probably suffered tectonic stress that created an internal deformation corridor with the same trend as important geological structures in the southern AO. These geological structures are interpreted by Alkimi et al. (2006) as features related to a lateral escape of the southernmost part of AO resulted in a dextral material transport along large dextral zones, resulting in features like the Guaçuí shear zone, near the Venda Nova. These authors claim that, during the final phases of the closure in the AO, the thickened northern half of the internal zone experienced extensional collapse, triggering igneous activity responsible for the creation of the post-orogenic features reported as the G5 supersuite of the collisional-subduction model. However, the observation that such collapse could have caused reactivations of these syn-orogenic zones have not been significantly discussed as an effect related to the emplacement of these plutonic bodies.

Bayer et al. (1987) mention that, although tectonic shearing is not evident in the Santa Angélica pluton, (i) a concentric concordant foliation, together with (ii) the position of triple points in the surrounding wallrocks near the contact with the pluton suggest an intrusion in a regional strain field caused by transcurrent shear. Ferreira de Souza-Junior et al. (2019) suggested that low-to-mid temperature features such as (i) monomineralic quartz-ribbons and (ii) bulgings associated to muscovite and chlorite paragenesis are related to a reactivation of a parallel branch of the GSZ in greenschist metamorphic facies probably due to the SA intrusion. We argued that, most likely, magmatic pulses arriving and accumulating at the magmatic chamber might have caused a reactivation of the anticline hinge (Fig. 11d) that Wiedemann et al. (2002) points as the emplacement structure for the Venda Nova in the final stages of its crystallization. That could explain an overall concentric pattern controlled by buoyance forces and a strictly constrained solid-state NE-SW deformation corridor printing a regional trend inside the pluton. The occurrence well-crystallized plagioclase grains with melting evidence on its borders and interstitial orthoclase (see section 4.1) might, in fact, be evidence of later hot pulses arriving in the last stages of the crystallization and causing the reactivation of such anticline.

The results of this paper corroborates with the observation of contrasting fabrics of southern and northern post-orogenic plutons of the AO. Temporim et al. (2020a) have shown that magnetic fabric of northern and shallower post-orogenic plutons of the Araçuaí Belt (e.g. Padre Paraíso charnockite, 502.7 ± 1.9 Ma, Xavier, 2017) have a N-S trending, coherent with the general trend of syn-orogenic country rocks. Such syn-tectonic-like fabric consistent with the gravity driven channel flow that controls the anatectic core of the AO (Cavalcante et al., 2013, 2014, 2018), could be a result of a still hot midcrust with slow cooling rates (3–5 °C/Ma) for the northern and hotter section of the AO, that resulted in temperatures near 500 °C around 510–500 Ma (Vauchez et al., 2019). In turn, coeval deep-seated intrusions in the colder flanks of the orogen present a concentric distribution of foliations and

lineations (Temporim et al., 2020a, 2020b), in stark contrast with the general NE-SW trend of the host rocks. In this scenario, VN is an example of the deep-seated intrusions of the south, with a major concentric fabric built by different magmatic pulses.

An important feature in the southern post-orogenic plutons is a clearer mantle involvement when compared to the northern ones (Fig. 12). Partial melts in the lower continental crust in orogens are not likely to produce melts through anatexis due a low H₂O at the H₂O-saturated-solidus, meaning that any melt remain in situ as a migmatite (Thompson and Connolly, 1995). If heat from lower basaltic magmas is added to the system, localized melts are more likely to develop (Huppert and Sparks, 1988). Gorczyk and Vogt (2018) have shown, through numerical modelling, that the thermal gradient controls ascent rate and the geometrical form of intrusions near the Moho. They verified as well that ascension is directly proportional to the vertical thermal gradient and that higher reliefs will produce flatter and lengthy intrusions, such as the northern batholiths of the AO. Gravity is, however, the main force to allow vertical rise of magmatic material through the continental crust, mainly through narrow conduits (Petford et al., 2000).

As previously argued by Wiedemann et al. (2002), once the asthenospheric mantle arises, heat is added to the base of the AO. Adiabatic decompression takes place in the rising mantle wedge, allowing mafic magma injection through early reactivated deep structures. Once hot basic magma arises, heat is quickly transferred to the surrounding crust enhancing new pulses of granitic/syenitic magma into the magmatic chamber. This mechanism would not only allow the formation of inversely zoned plutons found in the south of AO, putting together magmas from distinct sources in the same plutonic feature, but also to reactivate regional syn-orogenic structures and could even cause solid-state deformation inside the post-orogenic features, such as in the Venda Nova pluton.

6. Conclusions

The post-orogenic magmatism in the southern of the Araçuaí orogen is marked by the presence of inversely zoned plutons formed by felsic external facies composed mostly by granitic/syenomonzonitic rocks and gabbro-dioritic cores, eventually associated to charnockitic units. AMS data show that magnetic fabric is majorly concentric, with greater dip angles in the borders of the intrusion. AARM and coincidence of alignment of microstructures (such as feldspar orientation and deformational strips) corroborates to confirm a magnetic fabric controlled by MD magnetite. A high anisotropy corridor with solid-state deformation microstructures transects the pluton following the same trend as regional structures in southern AO. This feature conflicts with the major concentric magnetic pattern of the VN, possibly indicating that magnetite could have recorded paleostress caused by a reactivation of an antiformal hinge, as a consequence of the arrival of late pulses. Sub-magmatic deformation, distributed throughout the whole pluton, and indications of melting features in well-formed plagioclase grains of the mafic core support the hypothesis of intermittent contemporaneous pulses building this inversely zoned pluton. Charnockitic rocks in the western border of VN show a higher anisotropy degree and macroscopic solid-state deformational features, in which magnetic fabric dips towards the syenomonzonitic unit. These features reflect that charnockites are, in fact, a result of a previous pulse, later deformed by the intrusion of syenomonzonites and gabbros.

The tectonic trigger that probably caused the occurrence of these post-orogenic plutons could be related to the destabilization of the thick orogenic body, causing a reactivation of deep weak structures in the crust, like synform and antiformal hinges, through which the most felsic magmas of post-orogenic plutons intrude. Shifting to an extensional tectonic regime may have facilitated the ascension of the asthenospheric mantle, allowing the rise of the basic material that built the core of these inversely zoned plutons in southern AO.

Our data supports that a systemic evolution controlled the final

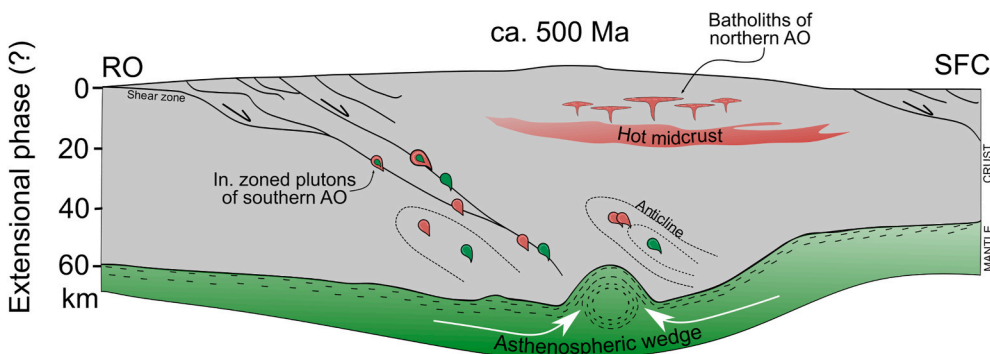


Fig. 12. Longitudinal (N-S) schematic representation of the AO around 500 Ma. In the right side is the northern orogenic limit with the São Francisco craton (SFC) bordering south with the limits of the Ribeira Orogen (RO). Diapiric intrusions through weak zones in crust of southern post-orogenic plutons are represented by pinkish (felsic material) and green (mafic magmas) forming the inversely zoned ballon-like plutons. (For interpretation of the references to colour in this figure legend, the reader is referred to the Web version of this article.)

phases of AO magmatism through pulses with varying temperatures within the same pluton, throughout its emplacement. The Venda Nova pluton, here interpreted as post-orogenic body, might actually record multi-stages of the bimodal magmatism triggered by a gravitational extensional collapse of the AO.

Declaration of competing interest

The authors declare that they have no known competing financial interests or personal relationships that could have appeared to influence the work reported in this paper.

Acknowledgements

This work has been performed at USPMag lab at Instituto de Astronomia, Geofísica e Ciências Atmosféricas (IAG) at the Universidade de São Paulo (USP), funded by CAPES/FAPESP/CNPq. Bellon also thanks the fellowship provided by the Coordenação de Aperfeiçoamento de Pessoal de Nível Superior - Brasil (CAPES), Finance Code 001. This study was supported by FAPESP (grant 2016/06114-6). We also would like to thank Haakon Fossen and Emilio Pueyo for the critical reviews that certainly helped to improve the quality of this paper.

Appendix A. Supplementary data

Supplementary data to this article can be found online at <https://doi.org/10.1016/j.jsg.2021.104401>.

Credit author statement

Ualisson Donardelli Bellon: Conceptualization, Methodology, Formal analysis, Investigation, Visualization, Writing – original draft. Manoel Souza D'Agrella Filho: Methodology, Investigation, Resources, Data curation, Supervision, Writing – review & editing. Filipe Altoé Temporim: Conceptualization, Methodology, Investigation, Writing – review & editing, Visualization. Gelson Ferreira de Souza Junior: Conceptualization, Formal analysis, Investigation, Visualization. Caroline Cibele Vieira Soares: Conceptualization, Investigation, Writing – review & editing, Supervision. Caio Augusto Deiroz Amaral: Investigation, Writing – review & editing. Lucas Pequeno Gouvêa: Investigation, Writing – review & editing. Trindade Ricardo Ivan Ferreira da: Conceptualization, Resources, Writing – review & editing, Supervision, Funding acquisition.

References

- Alkmim, F.F., 2015. Geological background: a tectonic panorama of Brazil. In: Vieira, B. C., Salgado, A.A.R., Santos, L.J.C. (Eds.), *Landscapes and Landforms of Brazil*. Springer Netherlands, Dordrecht, pp. 9–17. https://doi.org/10.1007/978-94-017-8023-0_2.
- Alkmim, F.F., Marshak, S., Pedrosa-Soares, A.C., Peres, G.G., Cruz, S.C.P., Whittington, A., 2006. Kinematic evolution of the Araçuaí-West Congo orogen in Brazil and Africa: nutcracker tectonics during the neoproterozoic assembly of

- Gondwana. *Precambrian Res.* 149, 43–64. <https://doi.org/10.1016/j.precamres.2006.06.007>.
- Alkmim, F.F., Pedrosa-Soares, A.C., Noce, C.M., Cruz, S.C.P., 2007. Sobre a evolução tectônica do orógeno Araçuaí-Congo ocidental. *Geonomos* 15, 25–43. <https://doi.org/10.18285/geonomos.v15i1.105>.
- Almeida, F.F.M., 1977. O cratão do São Francisco. *Rev. Bras. Geociências* 7, 349–364.
- Archanjo, C.J., Bouchez, J.L., 1997. Magnetic fabrics and microstructures of the post-collisional aegirine-augite syenite Triunfo pluton, northeast Brazil. *J. Struct. Geol.* 19, 849–860. [https://doi.org/10.1016/S0191-8141\(97\)00008-4](https://doi.org/10.1016/S0191-8141(97)00008-4).
- Archanjo, C.J., Hollanda, M.H.B.M., Rodrigues, S.W.O., Neves, B.B.B., Armstrong, R., 2008. Fabrics of pre- and syntectonic granite plutons and chronology of shear zones in the Eastern Borborema Province, NE Brazil. *J. Struct. Geol.* 30, 310–326. <https://doi.org/10.1016/j.jsg.2007.11.011>.
- Assumpção, M., Bianchi, M., Juliã, J., Dias, F.L., Sand França, G., Nascimento, R., Drouet, S., Pavao, C.G., Albuquerque, D.F., Lopes, A.E.V., 2013. Crustal thickness map of Brazil: data compilation and main features. *J. S. Am. Earth Sci.* 43, 74–85. <https://doi.org/10.1016/j.jsames.2012.12.009>.
- Bayer, P., Schmidt-Thomé, R., Weber-Diefenbach, K., Horn, H.A., 1987. Complex concentric granitoid intrusions in the coastal mobile belt, Espírito Santo, Brazil: the Santa Angélica Pluton - an example. *Geol. Rundsch.* 76, 357–371. <https://doi.org/10.1007/BF01821080>.
- Blenkinsop, T., 2000. Magmatic and sub-magmatic deformation. In: *Deformation Microstructures and Mechanisms in Minerals and Rocks*. Springer Netherlands, Dordrecht, pp. 59–64. https://doi.org/10.1007/0-306-47543-X_6.
- Borradaile, G.J., Henry, B., 1997. Tectonic applications of magnetic susceptibility and its anisotropy. *Earth Sci. Rev.* 42, 49–93. [https://doi.org/10.1016/S0012-8252\(96\)00044-X](https://doi.org/10.1016/S0012-8252(96)00044-X).
- Borradaile, G.J., Henry, B., 1996. Tectonic applications of magnetic susceptibility and its anisotropy. *Earth Sci. Rev.* 42, 49–93. <https://doi.org/10.1097/MJT.0b013e31824e2b9f>.
- Borradaile, G.J., Kehlenbeck, M.M., 1996. Possible cryptic tectono-magnetic fabrics in “post-tectonic” granitoid plutons of the Canadian Shield. *Earth Planet Sci. Lett.* 137, 59–64. https://doi.org/10.1007/978-94-017-1717-5_6.
- Bouchez, J.L., 1997. Granite is never isotropic: an introduction to AMS studies of granitic rocks. In: Bouchez, J.L., Hutton, D.H.W., Stephens, W.E. (Eds.), *Studies of Granitic Rocks Granite: from Segregation of Melt to Emplacement Fabrics*. Kluwer Academic Publishers, vol. 45. https://doi.org/10.1007/978-94-017-1717-5_6.
- Bouchez, J.L., Gleizes, G., Djouadi, T., Rochette, P., 1990. Microstructure and magnetic susceptibility applied to emplacement kinematics of granites: the example of the foix pluton (French pyrenees). *Tectonophysics* 184, 157–171. [https://doi.org/10.1016/0040-1951\(90\)90051-9](https://doi.org/10.1016/0040-1951(90)90051-9).
- Bridgwater, D., Sutton, J., Watterson, J., 1974. Crustal downfolding associated with igneous activity. *Tectonophysics* 21, 57–77. [https://doi.org/10.1016/0040-1951\(74\)90062-6](https://doi.org/10.1016/0040-1951(74)90062-6).
- Butler, R.F., 1992. Paleomagnetism: Magnetic Domains to Geologic Terranes, *Paleomagnetism: Magnetic Domains to Geologic Terranes*. <https://doi.org/10.5860/choice.29-5708>.
- Cavalcante, C., Fossen, H., Paes, R., Almeida, D., Helena, M., Hollanda, B.M., Egydio-silva, M., 2019. Reviewing the puzzling intracontinental termination of the Araçuaí-West Congo orogenic belt and its implications for orogenic development. *Precambrian Res.* 322, 85–98. <https://doi.org/10.1016/j.precamres.2018.12.025>.
- Cavalcante, C., Hollanda, M., Vauchez, A., Kawata, M., 2018. How long can the middle crust remain partially molten during orogeny? *Geology* 46, 839–842.
- Cavalcante, G.C.G., Egydio-Silva, M., Vauchez, A., Camps, P., Oliveira, E., 2013. Strain distribution across a partially molten middle crust: insights from the AMS mapping of the Carlos Chagas Anatectite, Araçuaí belt (East Brazil). *J. Struct. Geol.* 55, 79–100. <https://doi.org/10.1016/j.jsg.2013.08.001>.
- Cavalcante, G.C.G., Vauchez, A., Merlet, C., Egydio-Silva, M., De Holanda, M.H.B., Boyer, B., 2014. Thermal conditions during deformation of partially molten crust from TitanQ geothermometry: rheological implications for the anatexis domain of the Araçuaí belt, eastern Brazil. *Solid Earth* 5, 1223–1242. <https://doi.org/10.5194/se-5-1223-2014>.
- Cavalcante, G.C.G., Viegas, G., Archanjo, C.J., da Silva, M.E., 2016. The influence of partial melting and melt migration on the rheology of the continental crust. *J. Geodyn.* 101, 186–199. <https://doi.org/10.1016/j.jog.2016.06.002>.

- Day, R., Fuller, M., Schmidt, 1977. Hysteresis properties of titanomagnetites: grain-size and compositional dependence. *Phys. Earth Planet. In.* 13, 260–267. [https://doi.org/10.1016/0031-9201\(77\)90108-X](https://doi.org/10.1016/0031-9201(77)90108-X).
- De Campos, C.P., de Medeiros, S.R., Mendes, J.C., Pedrosa-Soares, A.C., Dussin, I., Ludka, I.P., Dantas, E.L., 2016. Cambro-ordovician magmatism in the Araçuaí belt (SE Brazil): snapshots from a post-collisional event. *J. S. Am. Earth Sci.* 68, 248–268. <https://doi.org/10.1016/j.jsames.2015.11.016>.
- De Campos, C.P., Mendes, J.C., Ludka, I.P., de Medeiros, S.R., de Moura, J.C., Wallfuss, C., 2004. A review of the Brazilian magmatism in southern Espírito Santo, Brazil, with emphasis on post-collisional magmatism. *J. Virtual Explor.* 17, 1–44. <https://doi.org/10.3809/jvirtex.2004.00106>.
- de Oliveira, D.C., Neves, S.P., Trindade, R.I.F., Dall'Agnol, R., Mariano, G., Correia, P.B., 2010. Magnetic anisotropy of the Redenção granite, eastern Amazonian craton (Brazil): implications for the emplacement of A-type plutons. *Tectonophysics* 493, 27–41. <https://doi.org/10.1016/j.tecto.2010.07.018>.
- Dunlop, J., Özdemir, O., 1997. *Rock Magnetism: Fundamentals and Frontiers*, first ed. Cambridge University Press, Cambridge.
- Ferreira de Souza-Junior, G., Soares, C.V.S., Temporim, F.A., Gouvêa, L.P., Trindade, R.I.F., 2019. Levantamento litostrostrual do segmento central da Zona de Cisalhamento Guaçuá. In: Jelinek, A.R., Guadagnin, F., Sommer, C.A., Souza, I.A., Soares Junior, A.V., Real e Silva, S., Kumaira, S. (Eds.), *Annals of the XI International Symposium on Tectonics*, p. 458.
- Fisher, R., 1953. Dispersion on a sphere. *Proc. Math. Phys. Eng. Sci.* 217, 295–305. <https://doi.org/10.1098/rspa.1953.0064>.
- Fitz Gerald, J.D., Stünitz, H., 1993. Deformation of granitoids at low metamorphic grade. I: reactions and grain size reduction. *Tectonophysics* 221, 269–297. [https://doi.org/10.1016/0040-1951\(93\)90163-E](https://doi.org/10.1016/0040-1951(93)90163-E).
- Fossen, H., Cavalcante, C., Konopásek, J., Meira, V.T., de Almeida, R.P., Hollanda, M.H. B.M., Trompette, R., 2020. A critical discussion of the subduction-collision model for the Neoproterozoic Araçuaí-West Congo orogen. *Precambrian Res.* 343 <https://doi.org/10.1016/j.precamres.2020.105715>.
- Fossen, H., Cavalcante, C.G., de Almeida, R.P., 2017. Hot versus cold orogenic Behavior: comparing. *Tectonics* 36, 2159–2178. <https://doi.org/10.1002/2017TC004743>.
- Gerya, T.V., Burg, J.P., 2007. Intrusion of ultramafic magmatic bodies into the continental crust: numerical simulation. *Phys. Earth Planet. In.* 160, 124–142. <https://doi.org/10.1016/j.pepi.2006.10.004>.
- Goodwin, L.B., Tikoff, B., 2002. Competency contrast, kinematics, and the development of foliations and lineations in the crust. *J. Struct. Geol.* 24, 1065–1085. [https://doi.org/10.1016/S0191-8141\(01\)00092-X](https://doi.org/10.1016/S0191-8141(01)00092-X).
- Gorczyk, W., Vogt, K., 2018. Intrusion of magmatic bodies into the continental crust: 3-D numerical models. *Tectonics* 37, 705–723. <https://doi.org/10.1002/2017TC004738>.
- Gradim, C., Roncato, J., Pedrosa-Soares, A.C., Cordani, U., Dussin, I., Alkmim, F.F., Queiroga, G., Jacobsohn, T., Da Silva, L.C., Babinski, M., 2014. The hot back-arc zone of the Araçuaí orogen, eastern Brazil: from sedimentation to granite generation. *Braz. J. Genet.* 44, 155–180. <https://doi.org/10.5327/Z2317-4889201400010012>.
- Harry, W.T., Richey, J.E., 1963. Magmatic pulses in the emplacement of plutons. *Geol. J.* 3, 254–268. <https://doi.org/10.1002/gj.3350030204>.
- Holder, M.T., 1979. An emplacement mechanism for post-tectonic granites and its implications for their geochemical features. *Origin of Granite Batholiths* 116–128.
- Horn, H.A., Weber-Diefenbach, W., 1987. Geochemical and genetic studies of three zoned intrusive bodies of both alkaline and calc-alkaline composition in the Ribeira Mobile Belt (Espírito Santo, Brazil). *Rev. Bras. Geociencias* 17, 488–497.
- Hrouda, F., Jelinek, V., Zapletal, K., 1997. Refined technique for susceptibility resolution into ferromagnetic and paramagnetic components based on susceptibility temperature-variation measurement. *Geophys. J. Int.* 129, 715–719. <https://doi.org/10.1111/j.1365-246X.1997.tb04506.x>.
- Hrouda, F., Schulmann, K., 1990. Conversion of the magnetic susceptibility tensor into the orientation tensor in some rocks. *Phys. Earth Planet. In.* 63, 71–77. [https://doi.org/10.1016/0031-9201\(90\)90061-2](https://doi.org/10.1016/0031-9201(90)90061-2).
- Huppert, H.E., Sparks, R.J., 1988. The generation of granitic magmas by intrusion of basalt into continental crust. *J. Petrol.* 29, 599–624. <https://doi.org/10.1093/petrology/29.3.599>.
- Jackson, M., 1991. Anisotropy of magnetic remanence: a brief review of mineralogical sources, physical origins, and geological applications, and comparison with susceptibility anisotropy. *Pure Appl. Geophys.* 136, 1–28. <https://doi.org/10.1007/BF00878885>.
- Jelinek, V., 1978. Statistical processing of anisotropy of magnetic susceptibility measured on groups of specimens. *Studia Geophys. Geod.* 22, 50–62. <https://doi.org/10.1007/BF01613632>.
- Konopásek, J., Cavalcante, C., Fossen, H., Janoušek, V., 2020. Adamastor – an ocean that never existed? *Earth Sci. Rev.* 205, 103201. <https://doi.org/10.1016/j.earscirev.2020.103201>.
- Liégeois, J.P., 1998. Preface — some words on the post-collisional magmatism. *Lithos* 45, xv–xvii.
- Ludka, I.P., Wiedemann, C.M., Töpfer, C., 1998. On the origin of incompatible element enrichment in the Venda Nova pluton, State of Espírito Santo, southeast Brazil. *J. S. Am. Earth Sci.* 11, 473–486. [https://doi.org/10.1016/S0895-9811\(98\)00028-5](https://doi.org/10.1016/S0895-9811(98)00028-5).
- Meert, J.G., Pivarunas, A.F., Evans, D.A.D., Pisarevsky, S.A., Pesonen, L.J., Li, Z., Elming, S., Miller, S.R., Zhang, S., Salminen, J.M., 2020. The magnificent seven: a proposal for modest revision of the Van der Voo (1990) quality index. *Tectonophysics* 790, 228549. <https://doi.org/10.1016/j.tecto.2020.228549>.
- Melo, M.G., Stevens, G., Lana, C., Pedrosa-Soares, A.C., Frei, D., Alkmim, F.F., Alkmim, L.A., 2017. Two cryptic anatectic events within a syn-collisional granulitoid from the Araçuaí orogen (southeastern Brazil): evidence from the polymetamorphic Carlos Chagas batholith. *Lithos* 277, 51–71. <https://doi.org/10.1016/j.lithos.2016.10.012>.
- Mendes, J.C., De Campos, C.M.P., 2012. Norite and charnockites from the Venda Nova Pluton, SE Brazil: intensive parameters and some petrogenetic constraints. *Geoscience Frontiers* 3, 789–800. <https://doi.org/10.1016/j.gsf.2012.05.009>.
- Nédélec, A., Bouchez, J.L., 2015. *Granites: Petrology, Structure, Geological Setting and Metallogeny*, first ed. Press, Oxford University, Oxford.
- Passchier, C.W., Trouw, R.A.J., 2005. *Microtectonics*. Springer, Berlin, Heidelberg. <https://doi.org/10.1007/3-540-29359-0>.
- Paterson, S.R., Fowler, T.K., 1993. Re-examining pluton emplacement processes. *J. Struct. Geol.* 15, 191–206. [https://doi.org/10.1016/0191-8141\(93\)90095-R](https://doi.org/10.1016/0191-8141(93)90095-R).
- Payacán, I., Gutiérrez, F., Gelman, S.E., Bachmann, O., Parada, M.A., 2014. Comparing magnetic and magmatic fabrics to constrain the magma flow record in La Gloria pluton, central Chile. *J. Struct. Geol.* 69, 32–46. <https://doi.org/10.1016/j.jsg.2014.09.015>.
- Pedrosa-Soares, A.C., De Campos, C.P., Noce, C., Silva, L.C., Novo, T., Roncato, J., Medeiros, S., Castañeda, C., Queiroga, G., Dantas, E., Dussin, I., Alkmim, F., 2011. Late neoproterozoic – cambrian granitic magmatism in the Araçuaí orogen (Brazil), the eastern Brazilian pegmatite province and related mineral resources. *Geological Society, London, Special Publications* 350, 25–51. <https://doi.org/10.1144/SP350.3>.
- Pedrosa-soares, A.C., Noce, C.M., Alkmim, F.F., Carlos, L., Babinski, M., Cordani, U., Castañeda, C., 2007. Orogênio Araçuaí: síntese do conhecimento 30 anos após Almeida 1977. *Geonomos* 15, 1–16. <https://doi.org/10.18285/geonomos.v15i1.103>.
- Pedrosa-Soares, A.C., Noce, C.M., Wiedemann, C.M., Pinto, C.P., 2001. The Araçuaí-West-Congo Orogen in Brazil: an overview of a confined orogen formed during Gondwanaland assembly. *Precambrian Res.* 110, 307–323. [https://doi.org/10.1016/S0301-9268\(01\)00174-7](https://doi.org/10.1016/S0301-9268(01)00174-7).
- Pedrosa-Soares, A.C., Wiedemann-Leonardos, C.M., 2000. Evolution of the Araçuaí belt and its connection to the Ribeira belt, eastern Brazil. In: Cordani, U., Milani, E.J., Thomaz, A., Campos, D.A. (Eds.), *Tectonic Evolution of South America*, pp. 265–285. <https://doi.org/10.13140/2.1.3802.5928>.
- Petford, N., Cruden, A.R., McCaffrey, K.J.W., Vigneresse, J.L., 2000. Granite magma formation, transport and emplacement in the Earth's crust. *Nature* 408, 669–673. <https://doi.org/10.1038/35047000>.
- Petitgirard, S., Vauchez, A., Egydio-Silva, M., Bruguier, O., Camps, P., Monié, P., Babinski, M., Mondou, M., 2009. Conflicting structural and geochronological data from the Ibituruna quartz-syenite (SE Brazil): effect of protracted “hot” orogeny and slow cooling rate? *Tectonophysics* 477, 174–196. <https://doi.org/10.1016/j.tecto.2009.02.039>.
- Pike, C.R., Roberts, A.P., Dekkers, M.J., Verosub, K.L., 2001. An investigation of multi-domain hysteresis mechanisms using FORC diagrams. *Phys. Earth Planet. In.* 126, 11–25. [https://doi.org/10.1016/S0031-9201\(01\)00241-2](https://doi.org/10.1016/S0031-9201(01)00241-2).
- Prior, D.J., 1993. Sub-critical fracture and associated retrogression of garnet during mylonitization. *Contrib. Mineral. Petrol.* 113, 545–556. <https://doi.org/10.1007/BF00698322>.
- Pueyo, E.L., Román-Berdiel, M.T., Bouchez, J.L., Casas, A.M., Larrasoña, J.C., 2004. Statistical significance of magnetic fabric data in studies of paramagnetic granites. *Geol. Soc. Spec. Publ.* 238, 395–420. <https://doi.org/10.1144/GSL.SP.2004.238.01.21>.
- Rosenberg, C.L., 2004. Shear zones and magma ascent: a model based on a review of the Tertiary magmatism in the Alps. *Tectonics* 23. <https://doi.org/10.1029/2003TC001526>.
- Sant’Ovaia, H., Bouchez, J.L., Noronha, F., Leblanc, D., Vigneresse, J.L., 2000. Composite-laccolitic emplacement of the post-tectonic Vila Pouca de Aguiar granite pluton (northern Portugal): a combined AMS and gravity study. *Trans. R. Soc. Edinb. Earth Sci.* 91, 123–137. <https://doi.org/10.1017/s026359330000732x>.
- Serrano, P., Pedrosa-Soares, A., Medeiros-Junior, E., Fonte-Boa, T., Araújo, C., Dussin, I., Queiroga, G., Lana, C., 2018. A-type Medina batholith and post-collisional anatexis in the Araçuaí orogen (SE Brazil). *Lithos* 320–321, 515–536. <https://doi.org/10.1016/j.lithos.2018.09.009>.
- Seymour, N.M., Singleton, J.S., Mavor, S.P., Gomila, R., Strockli, D.F., Heuser, G., Arancibia, G., 2020. The relationship between magmatism and deformation along the intra-arc strike-slip atacama fault system, northern Chile. *Tectonics* 39, 1–29. <https://doi.org/10.1029/2019TC005702>.
- Shea, W.L., Kronenberg, A.K., 1993. Strength and anisotropy of foliated rocks with varied mica contents. *J. Struct. Geol.* 15, 1097–1121. [https://doi.org/10.1016/0191-8141\(93\)90158-7](https://doi.org/10.1016/0191-8141(93)90158-7).
- Signorelli, N., 1993. *Folha Afonso Cláudio (Folha SF.24-V-A-II)*. Brasília.
- Tauxe, L., 2005. *Lectures in Paleomagnetism*, first ed.
- Tauxe, L., Mullender, T.A.T., Pick, T., 1996. Potbellies, wasp-waists, and superparamagnetism in magnetic hysteresis. *J. Geophys. Res.: Solid Earth* 101, 571–583. <https://doi.org/10.1029/95JB03041>.
- Tedeschi, M., Novo, T., Pedrosa-Soares, A., Dussin, I., Tassinari, C., Silva, L.C., Gonçalves, L., Alkmim, F., Lana, C., Figueiredo, C., Dantas, E., Medeiros, S., De Campos, C., Corrales, F., Heilbron, M., 2016. The Ediacaran Rio Doce magmatic arc revisited (Araçuaí-Ribeira orogenic system, SE Brazil). *J. S. Am. Earth Sci.* 68, 167–186. <https://doi.org/10.1016/j.jsames.2015.11.011>.
- Temporim, F.A., Bellon, U.D., Domeier, M., Trindade, R.I.F., Agrella-filho, M.S.D., 2021. Constraining the Cambrian drift of Gondwana with new paleomagnetic data from post-collisional plutons of the Araçuaí orogen, SE Brazil. *Precambrian Res.* 359, 106212. <https://doi.org/10.1016/j.precamres.2021.106212>.
- Temporim, F.A., Trindade, R.I.F., Tohver, E., Egydio-silva, M., Valim, T., 2020a. Strain Partitioning in a Collapsing Hot Orogeny. *European Geosciences Union*. <https://doi.org/10.5194/egusphere-egu2020-2986>.
- Temporim, F.A., Trindade, R.I.F., Tohver, E., Soares, C.C., Gouvêa, L.P., Egydio-Silva, M., Amaral, C.A.D., Souza, G.F., 2020b. Magnetic fabric and geochronology of a

- Cambrian “isotropic” pluton in the Neoproterozoic Araçuaí orogen. *Tectonics* 39, 1–21. <https://doi.org/10.1029/2019TC005877>.
- Thompson, A.B., Connolly, J.A.D., 1995. Melting of the continental crust: some thermal and petrological constraints on anatexis in continental collision zones and other tectonic settings. *J. Geophys. Res.* 100, 565–576. <https://doi.org/10.1029/95JB00191>.
- Trindade, R.I.F., Bouchez, J.L., Bolle, O., Nédélec, A., Peschler, A., Poitrasson, F., 2001. Secondary fabrics revealed by remanence anisotropy: methodological study and examples from plutonic rocks. *Geophys. J. Int.* 147, 310–318. <https://doi.org/10.1046/j.0956-540x.2001.01529.x>.
- Trompette, R., 1997. Neoproterozoic (~600 Ma) aggregation of western Gondwana: a tentative scenario. *Precambrian Res.* 82, 101–112. [https://doi.org/10.1016/s0301-9268\(96\)00045-9](https://doi.org/10.1016/s0301-9268(96)00045-9).
- Van der Voo, R., 1990. The reliability of paleomagnetic. *Tectonophysics* 184, 1–9.
- Vaucher, A., Hollanda, M.H.B., Monié, P., Mondou, M., Egydio-Silva, M., 2019. Slow cooling and crystallization of the roots of the Neoproterozoic Araçuaí hot orogen (SE Brazil): implications for rheology, strain distribution, and deformation analysis. *Tectonophysics* 766, 500–518. <https://doi.org/10.1016/j.tecto.2019.05.013>.
- Vernon, R.H., 2018. *Microstructures of Deformed Rocks. A Practical Guide to Rock Microstructure*. Cambridge University Press, pp. 228–352. <https://doi.org/10.1017/9781108654609.007>.
- Vernon, R.H., 2000. Review of microstructural evidence of magmatic and solid-state flow. *Vis. Geosci. Annu. Arch.* 5, 1–23. <https://doi.org/10.1007/s10069-000-0002-3>.
- Vernon, R.H., Williams, V.A., D’arcy, W.F., 1983. Grain-size reduction and foliation development in a deformed granitoid Batholith. *Tectonophysics* 92, 123–145. [https://doi.org/10.1016/0040-1951\(83\)90087-2](https://doi.org/10.1016/0040-1951(83)90087-2).
- Vieira, S.V., Menezes, R.G., 2015. *Geologia e Recursos Minerais do Estado do Espírito Santo: texto explicativo do mapa geológico e de recursos minerais*. Companhia de Pesquisa de Recursos Minerais-CPRM/Serviço Geológico do Brasil (Belo Horizonte), 1–289.
- Weinberg, R.F., Sial, A.N., Mariano, G., 2004. Close spatial relationship between plutons and shear zones. *Geology* 32, 377–380. <https://doi.org/10.1130/G20290.1>.
- Wiedemann, C.M., De Medeiros, S.R., Ludka, I.P., Mendes, J.C., Costa-de-Moura, J., 2002. Architecture of late orogenic plutons in the araçuaí-ribeira fold belt, southeast Brazil. *Gondwana Res.* 5, 381–399. [https://doi.org/10.1016/S1342-937X\(05\)70730-9](https://doi.org/10.1016/S1342-937X(05)70730-9).
- Xavier, B.C., 2017. *Relações Tectônicas no Setor Central da Faixa Araçuaí : Análise Estrutural por ASM e Geocronologia U/Pb e Lu/Hf*. Universidade de São Paulo.
- Xu, W., Zhao, Z., Dai, L., 2020. Post-collisional mafic magmatism: record of lithospheric mantle evolution in continental orogenic belt. *Sci. China Earth Sci.* 63, 13. <https://doi.org/10.1007/s11430-019-9611-9>.